iScience

CellPress
OPEN ACCESS

Article

Single-cell profiling of glial cells from the mouse amygdala under opioid dependent and withdrawal states

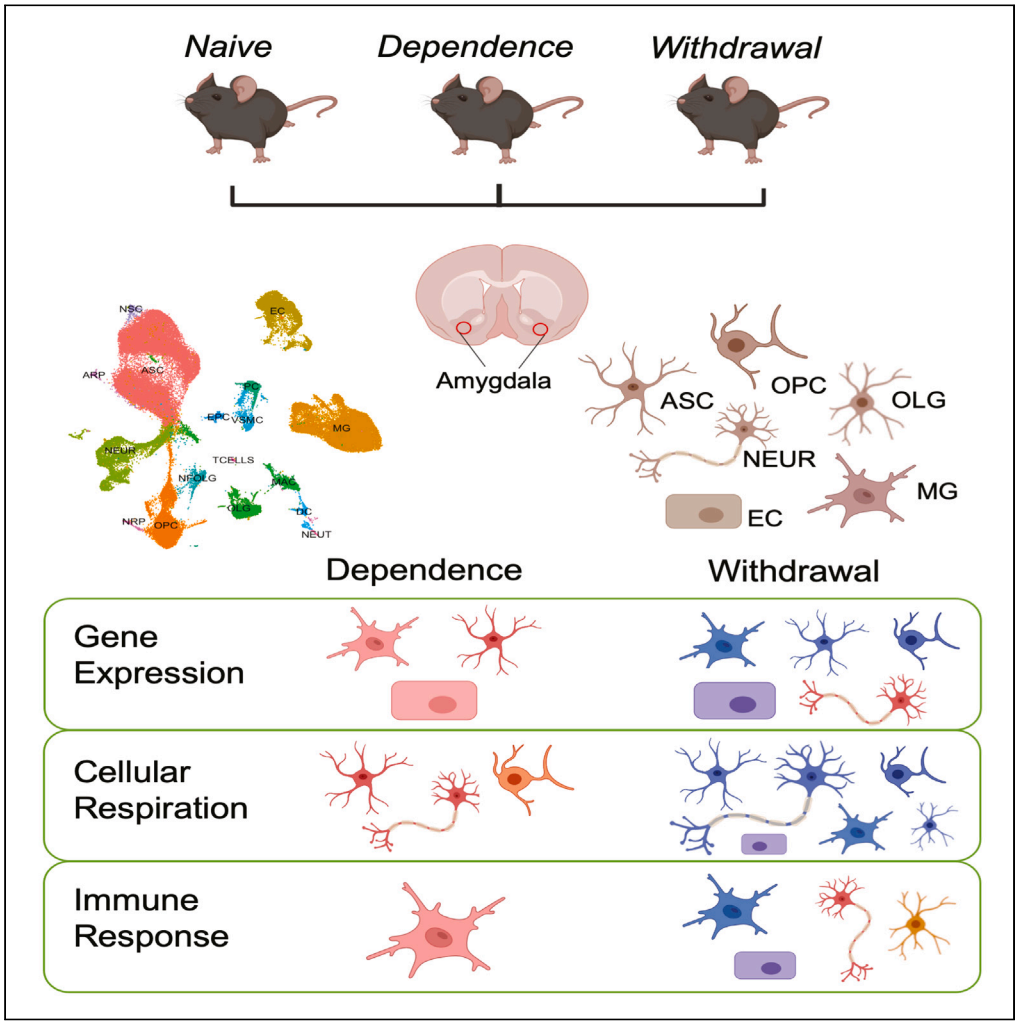

Yan Yan, Bridget Truitt, Junyi Tao, Sean Michael Boyles, Danielle Antoine, William Hulme, Sabita Roy

sabita.roy@miami.edu

Highlights

We have sequenced 121,856 cells in mouse amygdala with single cell RNA sequencing

This work has generated a comprehensive dataset for glial cell types during SUD

Key biological processes change in a cell type-specific manner

Dependence and withdrawal states showed significant difference at single cell level

Yan et al., iScience 26, 108166
November 17, 2023 © 2023
https://doi.org/10.1016/j.isci.2023.108166

iScience

CellPress
OPEN ACCESS

Article

Single-cell profiling of glial cells from the mouse amygdala under opioid dependent and withdrawal states

Yan Yan,[1] Bridget Truitt,[1] Junyi Tao,[1] Sean Michael Boyles,[2] Danielle Antoine,[1] William Hulme,[2] and Sabita Roy[1,3,*]

SUMMARY

The cycle of substance use disorder (SUD) leading to dependence is a complex process involving multiple neurocircuitries and brain regions. The amygdala is the core brain region that is involved in processing withdrawal and anxiety and depressive-like behaviors. However, the transcriptional changes in each cell type within the amygdala during SUD remains unknown. Here, we performed single-cell RNA sequencing and classified all cell types in the mouse amygdala. We particularly focused on gene expression changes in glial cells under dependent state and compared to either naive or withdrawal state. Our data revealed distinct changes in key biological processes, such as gene expression, immune response, inflammation, synaptic transmission, and mitochondrial respiration. Significant differences were unraveled in the transcriptional profiles between dependence and withdrawal states. This report is the first single-cell RNA sequencing dataset from the amygdala under opioid dependence and withdrawal conditions, providing unique insights in understanding brain alterations during SUD.

INTRODUCTION

Prevalence of substance use disorder (SUD) and associated deaths[1] have spurred efforts to develop new strategies for prevention or treatment of SUD. This requires improvement in our understanding of brain alterations during this complex, multistage process. It is well known that SUD is characterized by disturbances in several major neurocircuits that are driven by different brain regions: basal ganglia-driven intoxication stage, amygdala-driven withdrawal stage, and prefrontal cortex-driven anticipation stage.[2] However, there is a paucity of data at the molecular and cellular level of these brain regions at the single cell level. Previous studies applying bulk tissue preparations[3–6] have provided meaningful insights into SUD, but these data represented the changes in a mixture of cell populations. Cell type-specific information is highly important for us to understand the heterogeneous brain and to discover novel therapies that target specific genes/pathways in a specific cell population. Advances of the single-cell RNA sequencing (scRNA-seq) technology has enabled us to study thousands of cells belonging to different cell types simultaneously. A few studies have applied scRNA-seq to investigate different brain regions in SUD, including the nucleus accumbens (NAc) after acute morphine treatment,[7] and the prefrontal cortex (PFC) during cocaine addiction.[8] However, studies on the amygdala which mediates the negative affect during drug withdrawal[2] and modulates emotions such as anxiety and depression that occur as comorbidities of SUD,[9,10] are limited.

In this study, we analyzed the transcriptomic profiles of 77,957 individual cells from mouse amygdala. Distinct gene expression changes in different cell types under morphine dependence and withdrawal conditions were revealed. Our data suggest key biological processes and pathways are modulated in a cell-type specific manner following morphine dependence. Notably, significant changes of the cellular status were observed in the amygdala under morphine withdrawal state. We also investigated cell-cell communications under dependence and withdrawal states by analyzing ligand-receptor interactions that were modified under these two conditions. Since purification protocols that preserve glial viability are not optimum for neuron viability and since the procedure used in this study optimized glial isolation the data presented primarily focuses on glial cell transcriptomics and how activation of molecular pathways in the glial cells impact neighboring cell-cell interactions. These data will provide insight into our limited understanding of how the brain behaves during SUD, especially at the molecular and cellular levels. This study will also provide clues to develop novel preventative and therapeutic strategies for SUD.

[1]Department of Surgery, University of Miami Miller School of Medicine, Miami, FL 33136, USA
[2]John P. Hussman Institute for Human Genomics, University of Miami Miller School of Medicine, Miami, FL 33136, USA
[3]Lead contact
*Correspondence: sabita.roy@miami.edu
https://doi.org/10.1016/j.isci.2023.108166

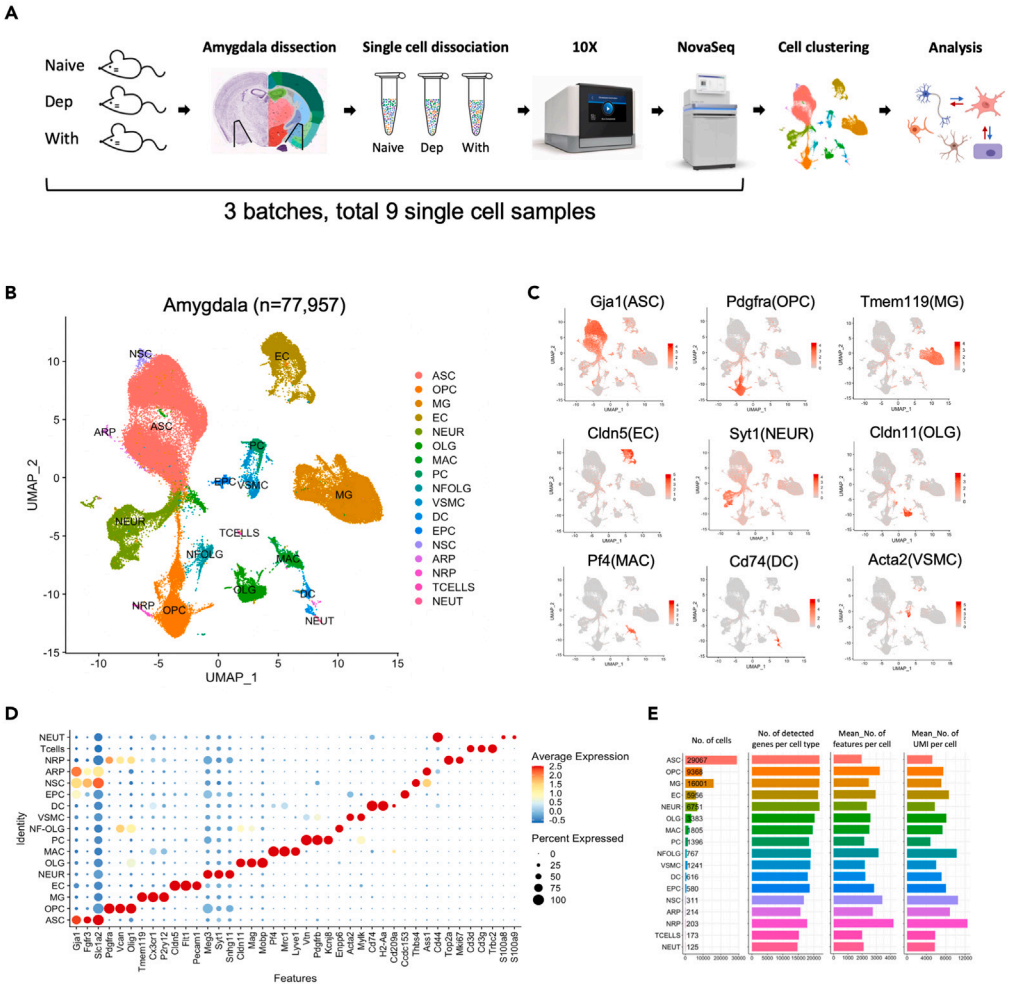

Figure 1. Identification of cell types in mouse amygdala

(A) Schematic of the experimental workflow. Naive: naive mice; Dep: mice under morphine dependence condition; With: mice under morphine withdrawal condition (see details in Figure S1A).

(B) UMAP (Uniform Manifold Approximation and Projection) plot showing the clustering of 77,957 cells (27141 from Naive, 27275 from Dep, 23541 from With) based on transcriptome. ASC, (astrocytes, *Gja1*$^{+}$), OPC (oligodendrocyte progenitor cells, *Pdgfra*$^{+}$), MG (microglial, *Tmem119*$^{+}$), EC (endothelial cells, *Cldn5*$^{+}$), NEUR (neurons, *Syt1*$^{+}$), OLG (oligodendrocytes, *Mobp*$^{+}$ or *Cldn11*$^{+}$), MAC (macrophages, *Pf4*$^{+}$), PC (pericytes, *Vtn*$^{+}$), NFOLG (newly formed oligodendrocytes, *Enpp6*$^{+}$), VSMC (vascular smooth muscle cells, *Acta2*$^{+}$), DC (dendritic cells, *Cd74*$^{+}$), EPC (ependymocytes, *Ccdc153*$^{+}$), NSC (neural stem cells, *Thbs4*$^{+}$), ARP (astrocyte-restricted precursors, *Cd44*$^{+}$), NRP (neuronal-restricted precursors, *Top2a*$^{+}$), T CELLS (T cells, *Cd3d*$^{+}$), and NEUT (neutrophils, *S100a9*$^{+}$).

(C) UMAP plots of 9 cell populations showing the expression of cell type-specific/enriched marker genes.

(D) Violin plot showing the expression of well-known cell type-specific/enriched marker genes in 17 cell clusters.

(E) Bar plots showing the number of cells, number of detected genes in each cluster, the average number of features (genes) and UMI counts in each cluster. See also Figures S1–S8, Tables S1, S2, S3, S6, and S8.

RESULTS

Identification of cell types in the amygdala

To study the mouse brain under different conditions of SUD, mice were treated with morphine sulfate for 7 days to induce dependence. In the withdrawal studies, morphine injection was stopped at day 7 for 24 h to induce spontaneous withdrawal (Figure S1A). As expected, the mouse body weight was reduced after morphine treatment (Figure S1B), and consistent with the withdrawal condition the mice exhibited withdrawal symptoms such as jumping and shaking (Figure S1C). We dissected the amygdalae from the naive (Naive), morphine dependent (Dep), and morphine withdrawal (With) mouse brains, after which the tissues were dissociated into single cell suspension. The cells were captured with the 10X Chromium platform, and the scRNA-seq was conducted to examine the transcriptomic profiles (Figure 1A).

We sequenced 121,856 cells from 9 independent biological samples, each of which was derived from pooled amygdalae from 4 to 5 mice in a single treatment group. We removed debris, dead cells, potential doublets, and unrecognized clusters (see STAR methods and

Figures S2 and S3). In the end, our analysis resulted in 77,957 high quality cells, representing 17 cell types (Figure 1B), with distinct expression profiles (Figures 1C and 1D). As shown in Figure 1E, the major cell types including neurons (NEUR), astrocytes (ASC), microglia (MG), oligodendrocyte progenitor cells (OPCs), and endothelial cells (EC), where more cells were captured and analyzed, the number of detected genes in these cell populations were higher than that in the small populations. It was in the stem cell/precursor cell types, including neural stem cells (NSC), neuronal-restricted precursors (NRP), and OPC, that we observed a higher average number of genes/UMI counts per cell.

The proportion of each cell type was consistent among the three experimental groups (Figures S3F and S3G). Although the estimated percentages might not reflect the actual composition of the amygdala since different cell types have different sensitivity to the dissociation procedure, these data suggested that the tissue composition of the amygdala remained unchanged after chronic morphine treatment. Median UMI per cell and the average number of detected genes were also consistent among the three groups (Figure S4). Other metrics are summarized in Table S2.

Identification of differentially expressed genes under morphine dependence and withdrawal conditions

We then analyzed the differentially expressed genes (DEG) to study the transcriptional changes in each cell type under the morphine dependence condition (Dep vs. Naive), and under the withdrawal condition following the dependence status (With vs. Dep). In both comparisons, each cell type exhibited distinct changes (Figures 2A, 2B, S5, and S6; Tables S4 and S5). Under the dependence condition, there were a greater number of upregulated genes than downregulated genes in particularly in the microglia, endothelial cells, neurons and OPC (Figure 2C). Compared to that in Dep vs. Naive, the numbers of DEG in With vs. Dep were almost doubled in most of the cell types (Figure 2D), suggesting that there were more significant changes in the amygdala when the brain switched from morphine dependence to withdrawal state.

The resident immune cells, microglia, showed very distinct changes (Figures 2E and 2F). When the overlapping relation between the DEGs under the two conditions were analyzed, we found that around 45% of the DEG under the dependence state were inversely correlated with the withdrawal state (Figure 2G). However, this inverse DEG counted for only a small percentage (~30%) of the DEG in the withdrawal state.

Next, we studied the DEG that were shared across the 17 cell types and found heat shock protein genes were on top of the DEG lists (Tables S4 and S5). As shown in Figure 2H, in most glia cell types Hsp90 family genes were downregulated, while the Hsp70 family (*Hspa1a*, *Hspa1b*) and Hsp40 family genes were upregulated under the dependence condition. However, in the withdrawal condition these heat shock proteins were mostly downregulated (Figure 2I). Since heat shock proteins play an important role in protein folding and stress response,[11] these data reveal how brain cells respond to the stresses associated with either chronic opioid use or opioid withdrawal in mice.

Identification of neuron and astrocyte subtypes

Neuron is a highly diverse population and could be classified by different criteria such as morphology and electrical properties. Here, based on the single cell transcriptome we identified 15 neuron subpopulations in amygdala, including 8 excitatory, 6 inhibitory neuron subtypes plus the immature neurons (Figure S7A). We found that excitatory neurons and inhibitory neurons exhibited significant transcriptional differences (Figure S7B; Table S6). In addition to neurons, we analyzed the subtypes of astrocyte, the largest glia population that support neuronal activity. As shown in Figures S8A and S8B, we identified five astrocyte subtypes (ASC_1 to 5). The largest ASC subtype, ASC_1, showed high expression levels of genes in phagocytosis, neurotransmission, ion and water transport, and immune activity, while the subtype ASC_3 showed very low level expression in these genes, particularly S100b, Mertk (phagocytosis), Agt (synapse plasticity), Slc7a10 and Gria2 (neuro-transmission), and the genes that are important in ion transport and water transport. Interestingly, in the withdrawal state a significantly higher percentage of ASC_3 was observed when compared to both Naive and Dep states (Figures S8C and S8D). It will be interesting to investigate the specific features and functions of these subtypes, and their different roles in SUD in future studies.

Validation of cell type-specific gene expression changes

Next, we sought to validate some of the cell type specific DEG by mRNA fluorescence *in situ* hybridization (FISH). As discussed before, some of the heat shock proteins such as *Dnaja1* showed distinct changes under the morphine dependence and withdrawal conditions (Figures 2H, 2I, and 3A). This was confirmed in microglia cells (*Tmem119*+) as shown in Figures 3B and 3C. In addition, we observed that the number of *Dnaja1* mRNA puncta was generally increased under dependence while decreased under the withdrawal condition in other cells (*Tmem119*-) in the amygdala. This observation verified our single-cell data showing that the changes of *Dnaja1* were shared by several glia cell populations (Figures 2H and 2I).

Ccl2 is one of the most potent microglia chemokines that attract cells involved in the immune or inflammatory response. Consistent with our single-cell data (Figure 3D), the independent FISH data showed that *Ccl2* mRNA expression was induced in the microglia cells with chronic morphine treatment but was reduced following 24-h morphine withdrawal (Figures 3E and 3F).

Next, we isolated the microglial cells from the amygdala and measured the mRNA expression levels of several immune related genes. As shown in Figure 3G, the genes encoding cytokines (*Tnf* and *Il1beta*) and Toll-like receptor *Tlr2* were upregulated under dependence but was subsequently decreased under the withdrawal condition. These data further validated our scRNA-seq data (Tables S4 and S5) which showed the up-regulation of *Tnf* under dependence and down-regulation of *Tlr2* and *Il1beta* under withdrawal. Next, we performed bulk RNA-seq of the isolated microglial cells from the amygdala. Due to the low amount of starting material (thousands of isolated microglia cells) and limited statistical power, much fewer DEGs were detected in the bulk RNA-seq data compared to the number of DEGs in the

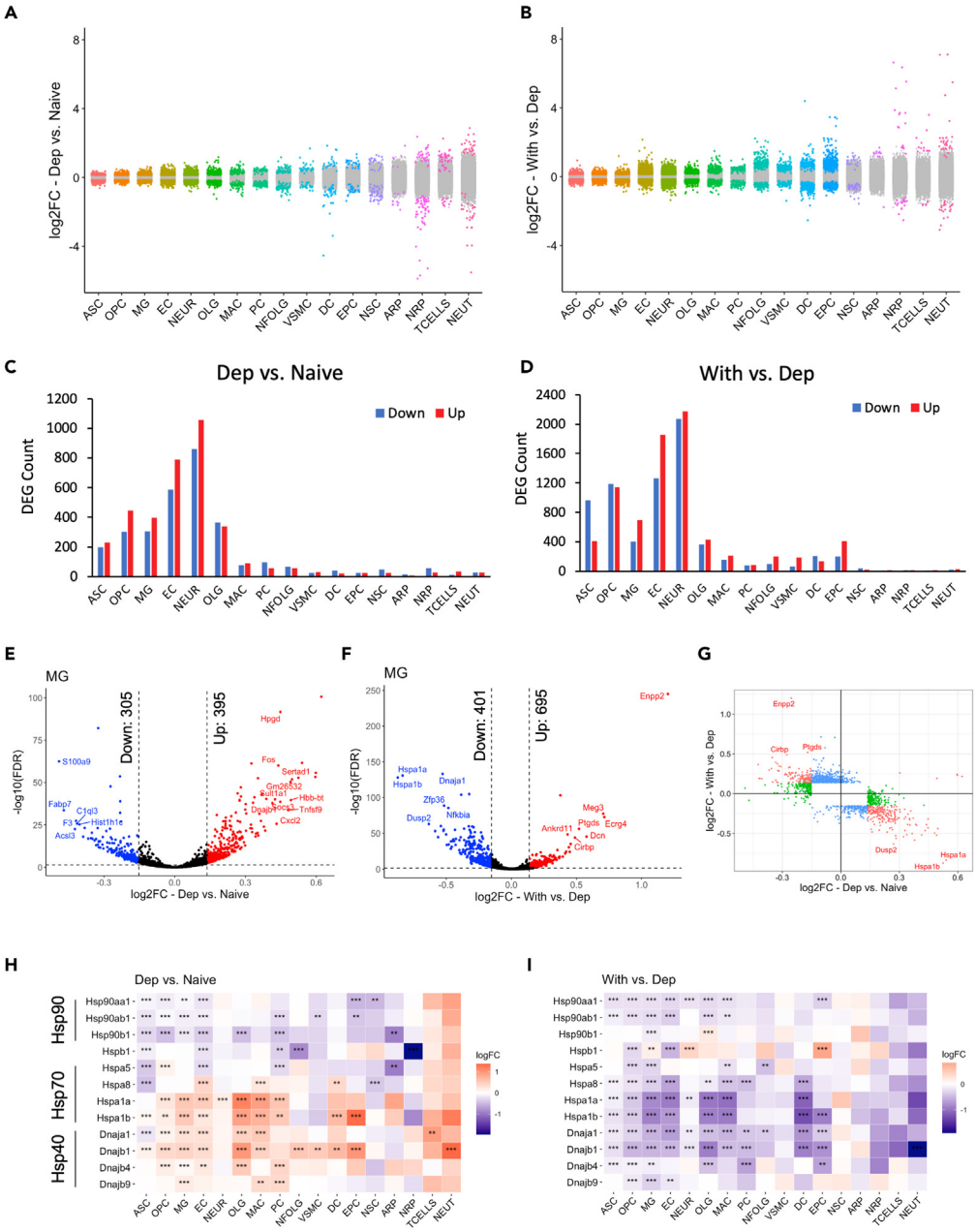

Figure 2. Differentially expressed genes under morphine dependence and withdrawal conditions

(A and B) Strip charts showing the logarithmic fold changes (log2FC) of all detected genes (dots) in 17 clusters. Genes in colored dots are significantly changed (FDR < 0.05 and FC > 10%) comparing Dep to Naive (A), or With to Dep (B).

(C, and D) Bar plots showing the number of significantly downregulated (Down) or upregulated (Up) genes in 17 clusters, comparing Dep to Naive (C), or With to Dep (D).

(E and F) Volcano plots showing the log2FC and -log10(FDR) of detected genes in MG, comparing Dep to Naive (E), or With to Dep (F). Significantly downregulated genes are dots in blue, upregulated genes are in red and genes in black are not significantly changed. (G) Dot plot showing the overlap (dots in red) of DEG in Dep vs. Naive (dots in green) with DEG in With vs. Dep (dots in blue) in MG.

(H and I) Heatmaps showing the log2FC of heat shock protein expressions comparing Dep to Naive (H), or With to Dep (I) in 17 clusters. * FDR < 0.05, ** FDR < 0.01, *** FDR < 0.001. See also Figures S5 and S6, Tables S4, S5, and S7.

scRNA-seq data (Figure S9). But there was a positive correlation of the gene expression fold changes between these two datasets (Figure 3H). This observation suggests that scRNA-seq might be a powerful tool to study the cell populations or samples that have limited cell numbers for bulk RNA-seq.

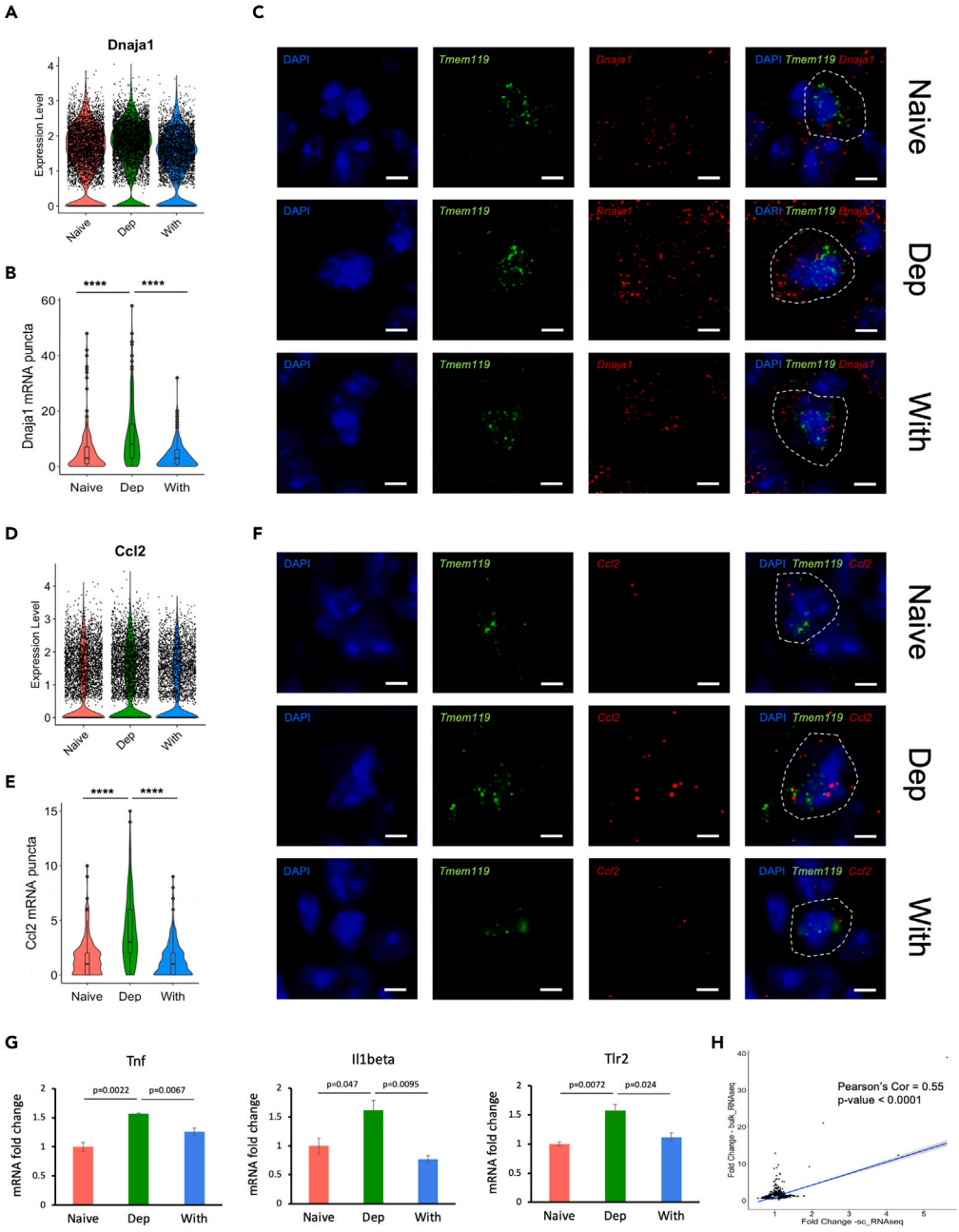

Figure 3. Validation of single-cell RNA sequencing data in microglia cells

(A) Violin plot overlaid with dot plot showing the expression levels of *Dnaja1* in our scRNA-seq data of MG population.

(B) Violin plot overlaid with boxplot showing the quantification of the RNAscope data. Data represent median expression of *Dnaja1* (number of mRNA puncta) in *Tmem119*$^{+}$ MG cells (n = 249 cells from 5 Naive mice, n = 280 cells from 5 Dep mice, n = 288 cells from 5 With mice). **** p value < 0.0001 by Mann-Whitney U-test.

(C) Representative RNAscope images of mouse amygdala showing the *Dnaja1* mRNA puncta in *Tmem119*$^{+}$ MG cells. Dotted lines outline the area of each cell that was considered for quantification. Scale bars, 5 μm.

(D) Violin plot overlaid with dot plot showing the expression levels of *Ccl2* in our scRNA-seq data of MG population.

(E) Violin plot overlaid with boxplot showing the quantification of the RNAscope data. Data represent median expression of *Ccl2* (number of mRNA puncta) in *Tmem119*$^{+}$ MG cells (n = 291 cells from 5 Naive mice, n = 303 cells from 5 Dep mice, n = 313 cells from 5 With mice). **** p value < 0.0001 by Mann-Whitney U-test.

(F) Representative RNAscope images of mouse amygdala showing the *Ccl2* mRNA puncta in *Tmem119*$^{+}$ MG cells. Scale bars, 5 μm.

(G) qPCR analysis of *Tnf*, *Il1beta*, and *Tlr2* in MG cells isolated from the amygdala of Naive, Dep and With mice. p values were analyzed by two tailed Student's *t* test. Data represent mean ± SEM of independent triplicate measurements.

(H) Scatterplot of the fold changes of the DEGs in the bulk RNA-seq dataset (isolated microglia cells) and scRNA-seq dataset (MG population). Linear regression is depicted with the blue line. Pearson's correlation coefficient and p value are shown in the plot. See also Figure S9.

Changes in distinct biological processes in neurons and microglial cells under morphine dependence and morphine withdrawal states

Next, we conducted a gene set enrichment analysis (GSEA)[12] to investigate the changes of various gene sets or pathways in each cell population and constructed an enrichment map[13] of the most significantly changed gene ontology terms (GOs) (Figures 4A and 4B). Microglia, as the resident immune cells in the brain, plays a pivotal role in the immune response and neuroinflammation.[14] Their activity is linked to various emotions and behaviors such as compulsive behaviors, anxiety, depression, and SUD.[15–18] Our GSEA data showed that 1143 biological process GOs were significantly changed (947 upregulated, 196 downregulated) under morphine dependence, while there were more deactivated GOs (468 upregulated, 1026 downregulated) when comparing the withdrawal state to dependence (Table S9 and S10). Consistent with our current understanding of opioid induced neuroinflammation[15,19,20] and microglia activation during opioid treatment,[21,22] in the morphine dependent microglia, the cell activation pathways were enhanced and the immune response, inflammatory response, cytokine production as well as the response to cytokines were upregulated (Figure 4A). The pathways involved in metabolic processes and gene expression were also activated. In agreement with the literature,[21,23,24] our data showed that chronic opioid treatment resulted in microglial apoptosis, and enhanced MAPK as well as ERK pathways. However, as shown in Figure 4B, under the withdrawal condition these activated pathways were mostly downregulated, suggesting a switch of the cellular status when the brain underwent the withdrawal process. Importantly, cellular responses to stress including the immune response, response to ROS, protein folding, etc. were deactivated, which was consistent with our DEG analysis showing a significant decrease in the expression of the heat shock protein families under the withdrawal condition (Figure 2I).

Distinct pathway changes across 17 different cell types

GSEA is more sensitive than the DEG analysis because it aggregates information from a set of genes which are functionally relevant, therefore we were able to conduct GSEA in all the cell types including the populations that had limited cell numbers and didn't show many DEGs. Under both dependence and withdrawal conditions, there were shared and cell type-specific changes of gene sets across the 17 cell types (Tables S9 and S10). Here we compared the GO terms that represented the key biological processes between different conditions (Figure 4C). With chronic morphine treatment the GSEA-predicted upregulated translation process and peptide biosynthesis were shared in astrocytes, microglia, oligodendrocytes (OLG), endothelial cells, and OPC. Cellular respiration pathways were shown in GSEA to be activated in neurons, astrocytes, newly formed oligodendrocyte (NFOLG) and OPC. Biosynthesis of different molecules and various cell signaling pathways exhibited distinct changes among 17 cell types. As shown here (Figure 4C-left) and discussed before, microglia was the major cell type that increased the immune/inflammatory response and cytokine production under dependence condition.

Compared to these dependent cells (Dep vs. Naive), the withdrawal cells (With vs. Dep) showed more significant changes (Figure 4C-right). Gene expression GOs and cellular respiration pathways were downregulated in the glia cells (ASC, OPC, MG, EC, OLG, etc.). Interestingly, two groups of cell types showed opposite changes in the immune related GOs: endothelial cells and immune cell types—microglia, macrophages, dendritic cells (DC), exhibited downregulation; while neurons, oligodendrocytes, ependymocytes (EPC), and NFOLG showed upregulations (discussed later). In addition, neurotransmitter transport was enhanced in microglia, dendritic cells, endothelial cells, ependymocytes, and NFOLG, but was deactivated in neuron and pericytes (PC).

Distinct and significant changes in immune response and inflammation in cell type specific manner

Among the biological processes being analyzed, immune response related pathways showed the most exciting changes as shown in Figure 4C. Neuroinflammation is involved in neurodegeneration diseases and neuronal disorders such as anxiety and SUD.[6,25,26] So next, we analyzed the detailed GO terms and pathways that were relevant to the immune response and inflammation. As shown in Figure 5A-left, when we compared the morphine dependent cells to naive cells, most of the activated pathway occurred in microglia.

More interesting and unexpected changes happened under the withdrawal condition (Figure 5A-right) when these cell populations were divided to two groups based on their immune status changes: group1 cell types (MG, MAC, DC, and EC) showed deactivations, however, group2 cell types (NEUR, OLG, NFOLG, and EPC) showed largely upregulations. All the group1 cell types showed downregulated GO terms including innate immune response, humoral immune response, inflammatory response, response to cytokines, and TNF production. In contrast, the group2 cell types shared upregulated immune response and cytokine productions, especially IL6 and interferon gamma production. The inflammatory response and TNF production were enhanced in most of these cell types.

Next, we checked for changes in inflammation related genes. As shown in Figure 5B, chronic morphine treatment induced the expression of *Ccl2*, *Cx3cl1*, *Gls*, *Tlr4*, and *Tnf* in the three immune cell populations—microglia, macrophages, and dendritic cells endothelial cells and macrophages showed a significant upregulation of *Icam1* and *Vcam1*, both of which encoded intercellular adhesion proteins that regulate immune cell recruitment to the sites of inflammation.

Under the withdrawal condition, the group1 immune cells showed decreased expression of *Nlrp3*, *Tlr4*, *Tnf*, *Hmox1* and several CC chemokine family members. *Icam1* and *Vcam1* expression were reduced in endothelial cells (Figure 5C). However, the group2 cells exhibited mostly the opposite changes (Figure 5D). For example, CC chemokine family members (*Ccl12*, *Ccl2*, *Ccl4*) and glutamate metabolism genes (*Gls*, *Glul*) were upregulated in ependymocytes and NFOLG. The induced expression of *Cx3cr1*, *Cxcl12*, *Tnf*, etc., were shared in group2 cell types.

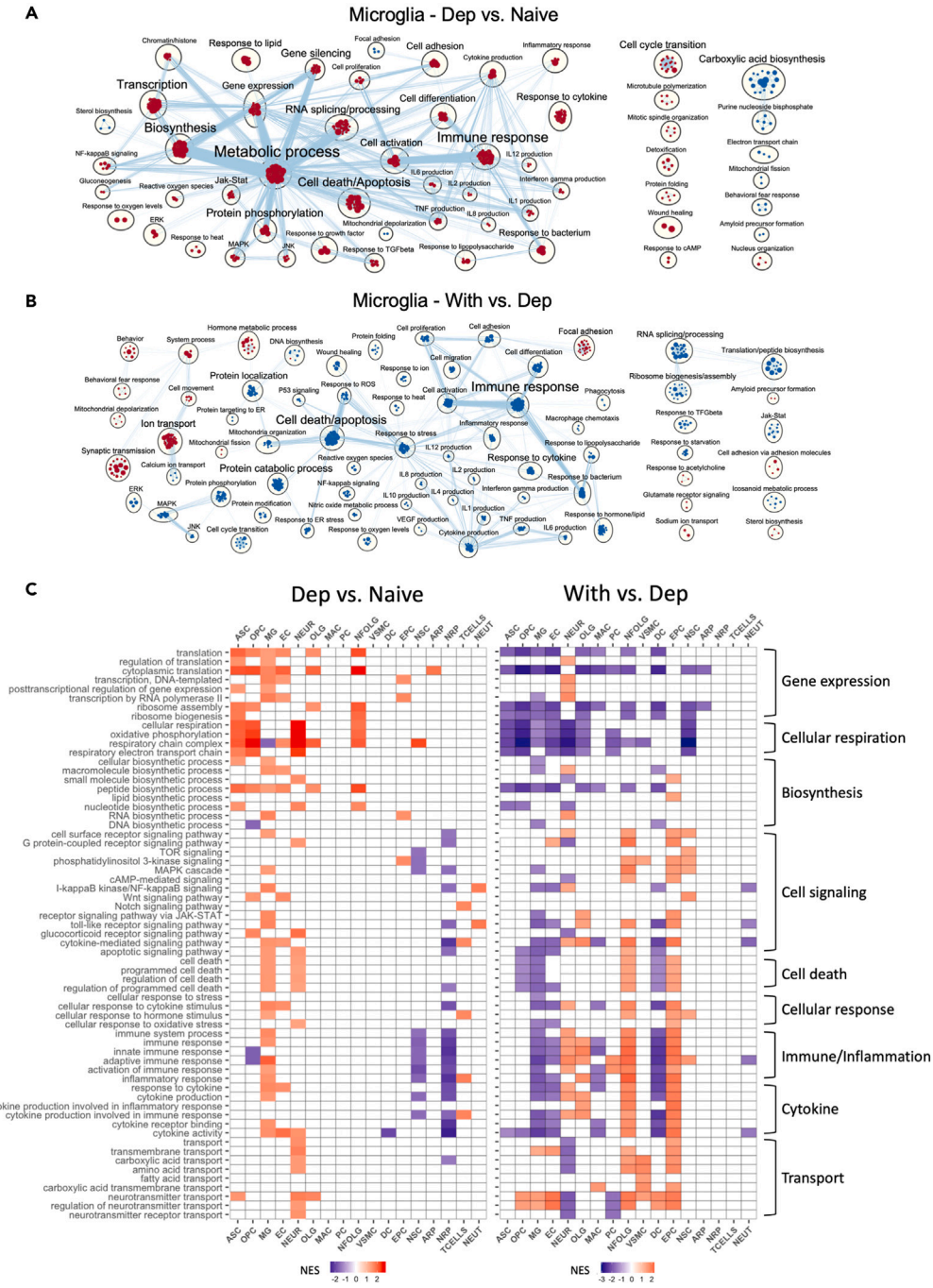

Figure 4. Changes in biological pathways and processes under morphine dependence and withdrawal conditions

(A and B) Enrichment maps of significant pathways (p value < 0.05 and FDR q value < 0.15) in MG comparing Dep to Naive (A), or With to Dep (B). Normalized enrichment scores (NES) were calculated for each pathway by GSEA. The networks were created using EnrichmentMap Cytoscape application. Pathways are shown as nodes which are colored by the corresponding NES, and edges represent the number of genes overlapping between two pathways. Clusters of nodes were labeled using the AutoAnnotate Cytoscape application to identify major biological themes. Positive NES (red nodes) indicate upregulation, while negative NES (blue nodes) indicate downregulation.

(C) Heatmap of NES showing a subset of significant pathways (p value < 0.05 and FDR q value < 0.25) in 17 cell types comparing Dep to Naive (left), or With to Dep (right). Positive NES indicates upregulation, negative NES indicates downregulation and white indicates no significant change. See also Tables S9 and S10.

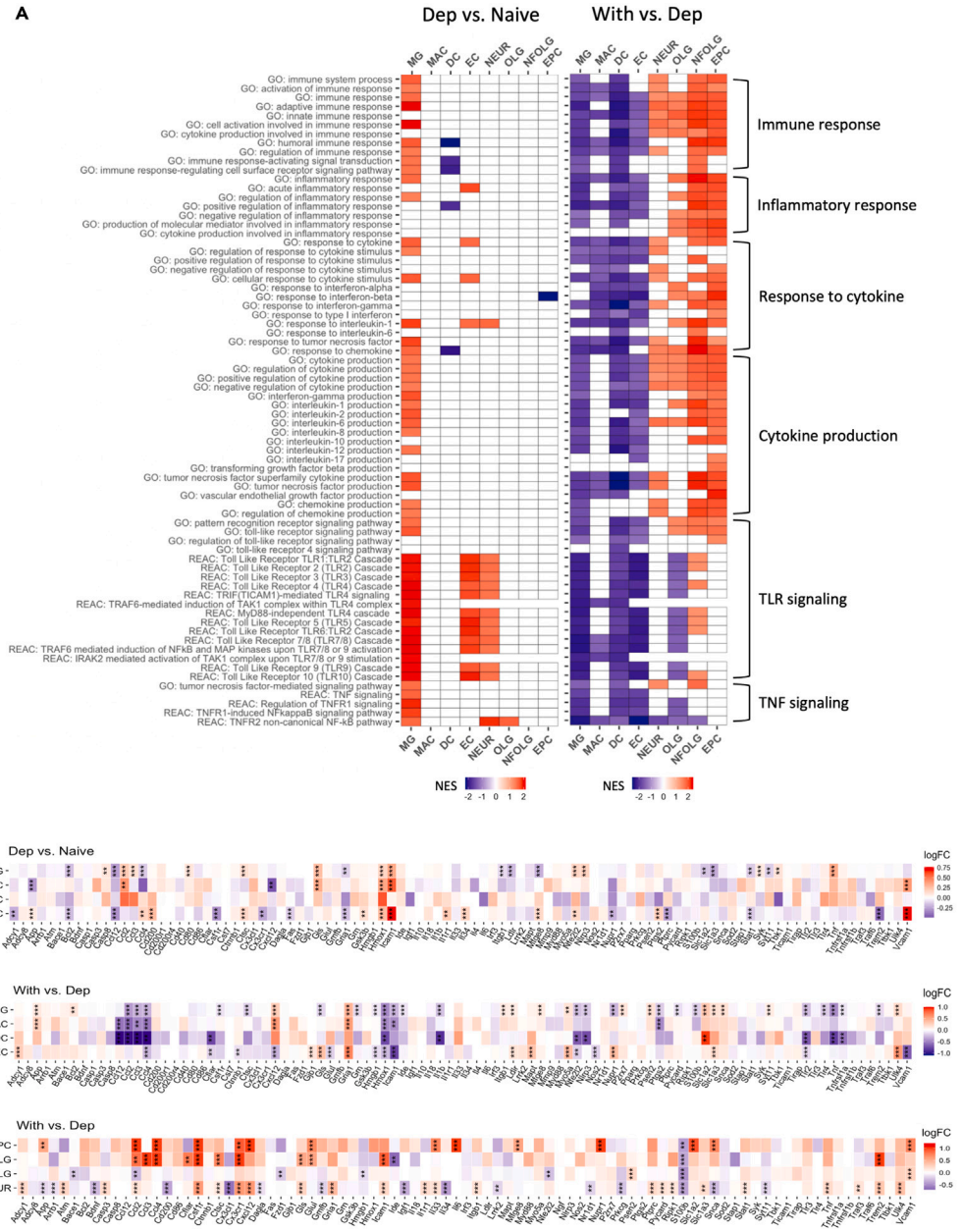

Figure 5. Changes in immune/inflammation related pathways and genes under morphine dependence and withdrawal conditions

(A) Heatmap of NES showing a subset of immune/inflammation related significant pathways (p value < 0.05 and FDR q value < 0.25) in 8 cell types comparing Dep to Naive (left), or With to Dep (right). Positive NES indicates upregulation, negative NES indicates downregulation, and white indicates no significant change.

(B) Heatmap showing the log2FC of inflammation related gene expressions comparing Dep to Naive in MG, MAC, DC, EC.

(C and D) Heatmaps showing the log2FC of inflammation related gene expressions comparing With to Dep in MG, MAC, DC, EC (C), and in EPC, NFOLG, OLG, NEUR (D). * FDR < 0.05, ** FDR < 0.01, *** FDR <0.001. See also Tables S9 and S10.

Changes in cell-cell communications after chronic morphine treatment

Finally, we analyzed the cell-cell interactions (CCI) among all the recognized cell types in the amygdala (see STAR methods). Based on the DEG analysis, we were able to study the changes of ligand-receptor/signaling interactions with chronic morphine treatment. Under the morphine dependence condition, we highlighted the communications among neurons, microglia, endothelial cells, and astrocytes. As shown in Figure 6, the increased expression of *Tnf* in MG possibly enhanced the interactions between microglia and neurons, or microglia and endothelial cells through a variety of receptors or pathways in neurons or endothelial cells. Importantly, this same ligand might regulate different biological processes, depending on the receptors. For example, microglia-*Tnf* can interact with several receptors on neurons (Figure 6A) and

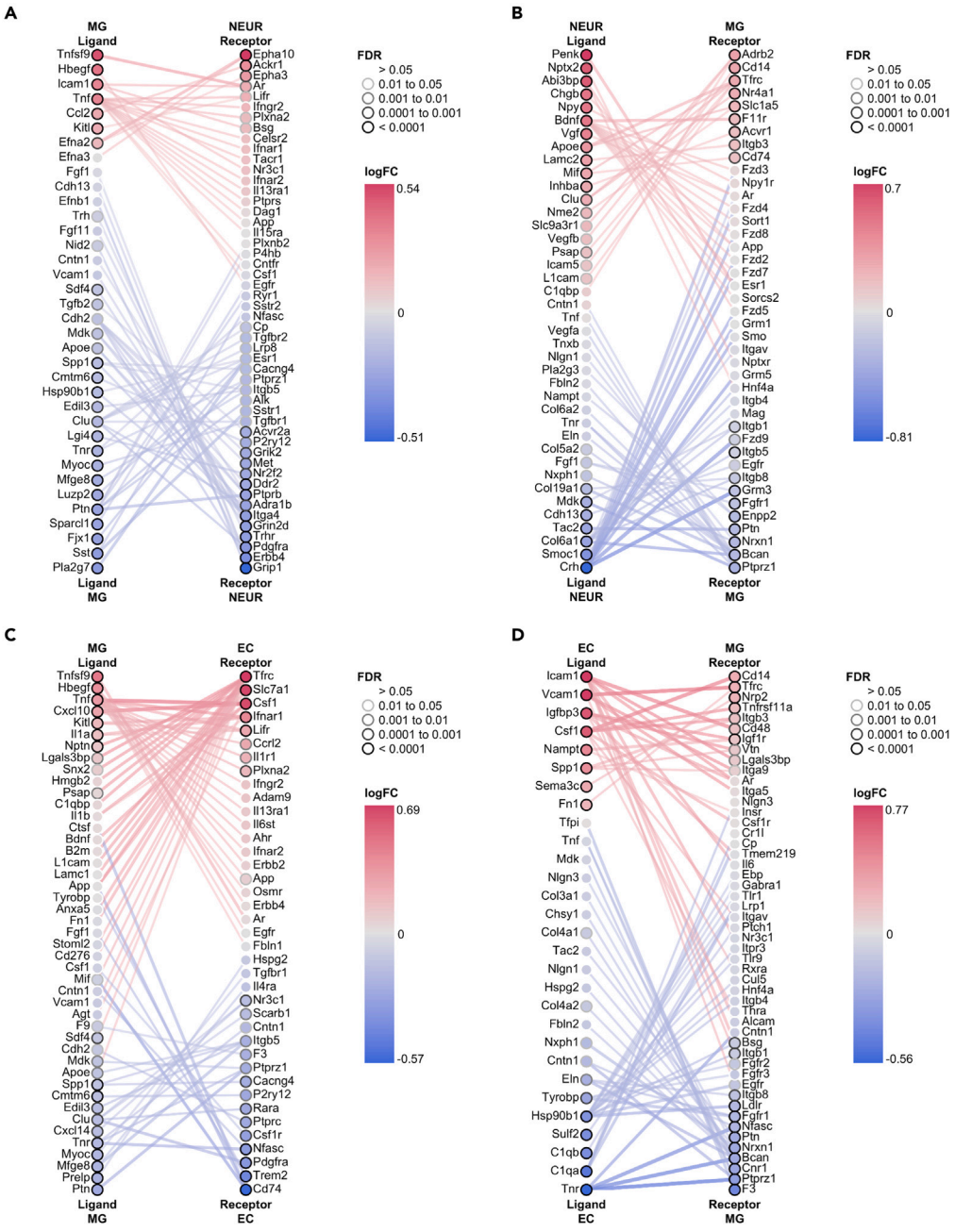

Figure 6. Changes in cell-cell interactions with chronic morphine treatment

Ligands or receptors in the denoted cell type are represented by the nodes which are colored by the log2FC. Node borders indicate the FDR value of the DEG analysis. Edges represent ligand-receptor interactions. Edge color indicates the sum of scaled differential expression magnitudes from the ligand node and receptor node. The Figures have been filtered so that the top 75 edges representing the most differentially expressed node pairs are shown. The comparisons were between Dep and Naive samples.

(A) Ligands expressed in MG with receptors expressed in NEUR.

(B) Ligands expressed in NEUR with receptors expressed in MG.

(C) Ligands expressed in MG with receptors expressed in EC.

(D) Ligands expressed in EC with receptors expressed in MG. See also Figure S10.

such as *Lifr* which has been shown to regulate neuron differentiation and maturation.[27] At the same time, *Tnf* upregulation in microglia can induce *Csf1* expression in endothelial cells (Figure 6C), and increased EC-*Csf1* can communicate with several pathways in the microglia (Figure 6D). For example, Csf1-Csf1 receptor (*Csf1r*) interaction is important for microglial viability and activity.[28] Endothelial cells also use other ligands to send signals back to microglia. The significantly upregulated *Vcam1* and *Spp1* in endothelial cells can potentiate the recruitment of microglia to the inflammatory site through binding to the increased receptor *Itga9* on microglial cells (Figure 6D).

In addition to the cell-cell interactions in different cell types, our single-cell data also revealed cell-cell interactions within the same cell type. BDNF, one of the neurotrophin family of growth factors, plays pivotal roles in neural growth, survival, plasticity and importantly, is involved in mood modulation and drug addiction.[29,30] Our current analysis showed that the increased *BDNF* expression in neurons, not only promoted its interactions with a variety of receptors on microglia (Figure 6B) and astrocytes (Figure S10B), but also activated its downstream signaling within the neuron population itself (Figure S10A).

Changes in cell-cell communications under morphine withdrawal

Under the withdrawal condition, a significant change was observed in cell-cell interactions when compared to the dependence state (Figures 7 and S11). Most of the activated interactions between microglia and endothelial cells under the dependence condition were downregulated (Figures 7A and 7B). Various cytokine-receptor mediated interactions were reduced, which might contribute to the dampened inflammatory responses in both microglia and endothelial cells under the withdrawal condition. The signals that microglia received, and decreased microglial activation may be a consequence of neuronal activation status. Both the reduced *Cxcl10* in endothelial cells (Figure 7B) and reduced *Cx3cl1* in neurons (Figure S11A) can possibly deactivate the Ccrl2 mediated pathway in microglia, which was important for microglial activation and polarization.[31]

Oligodendrocytes produce myelin sheaths that provide support and insulation to neurons, and ependymocytes play pivotal roles in cerebrospinal fluid homeostasis and brain metabolism. Our cell-cell interactions analysis revealed oligodendrocyte-neuron and ependymocyte-neuron interactions that may also regulate neuron growth and the immune response. As shown in Figures 7C, 7D, and S11C, the increased expression of ligands including *Vtn*, *Fn1*, and *Spp1* in oligodendrocytes, ependymocytes, and NFOLG would enhance their interactions with the receptor *Itga8*, which was also significantly increased in neurons and was involved in neurite outgrowth.[32] Several cytokine receptors (*Il1rap*, *Cx3cr1*, *Il6ra*, etc.) were upregulated in neurons, and their corresponding ligands (*Il1a*, *Cxcl10*, *Il6*, etc.) were expressed at increased levels in oligodendrocytes and ependymocytes; therefore, the interactions between these ligands and receptors most likely will promote immune responses in neurons. Notably, since the cytokine productions were reduced in microglia, dendritic cells, and endothelial cells under morphine withdrawal (Figures 5A and 5C), the enhanced cytokine signals that neurons received might mainly come from the non-immune glial cells, oligodendrocytes, and ependymocytes.

In summary, our single-cell data unraveled gene expression and pathway changes that regulated key biological processes within each cell population and in other cell types via modified cell-cell communications.

DISCUSSION

SUD is a complex process in which various brain regions are involved. The amygdala is a recognized region that mediates the withdrawal effect as well as anxiety and depression-like behaviors, both of which are well known co-morbidities of SUD.[2,9,10] In this study, we performed scRNA-seq to identify the cell types in mouse amygdala and investigated their unique transcriptional profiles under both morphine dependence and withdrawal states. Since our purification protocol primarily is optimized for glial cell isolation, data presented focused on the microglial population and its interactions with other cell types including the neuronal population.

As was observed in other scRNA-seq studies investigating the whole brain and other brain regions,[7,8,33] the mouse amygdala also showed rich cellular heterogeneity. Our study identified 17 major cell types (Figure 1B), and subtypes for neurons and astrocytes (Figures S7 and S8). The proportion of each cell type was consistent, suggesting chronic morphine treatment did not influence the composition of the amygdala tissue, but did affect the transcriptional profiles of all cell types according to our subsequent DEG analysis.

When we compared the morphine dependence sample to the naive sample, different cell types exhibited distinct transcriptional changes (Figures 2A, 2E, and S5). When the condition switched to withdrawal, most of the cell populations showed more significant DEG (Figure 2D). Interestingly, the neuronal population exhibited the most prominent changes under the withdrawal state. These data are in line with the study showing that transcriptional changes in the PFC neurons were more significant during cocaine withdrawal than that during the drug maintenance phase.[8] These imply the importance of the cellular response to withdrawal-induced stimuli in the development of drug dependence.

Heat shock proteins play important roles in protein folding and cellular response to stress.[11] Hsp70 and Hsp40 families were largely upregulated under the morphine dependence condition (Figure 2H), which was consistent with other studies showing that morphine exposure induced the expression of Hsp70 and Hsp40 mRNAs in various brain regions such as the frontal cortex and amygdala.[34,35] Considering the role of Hsp70 in cell survival, the function of Hsp40 as the co-chaperone for Hsp70 and their interactions with the MAPK signaling pathways,[36,37] it is likely that the upregulation of these heat shock proteins reflects a protective effect against morphine-induced cell toxicity which has been reported by other research groups.[23,24] This is also illustrated in our single-cell data with the increased cell death which was predicted by GSEA and activated MAPK as well as ERK signaling in glial cells, like microglia (Figure 4A). In addition, our current data (Figure 2I) and data by Ammon et al. showed the morphine treatment-induced Hsp70 and Hsp40 were reversed under spontaneous withdrawal as well as under naloxone-precipitated withdrawal.[35] Future studies on the dynamic changes of these heat shock proteins will reveal more information about how the cells respond to stresses under different SUD states.

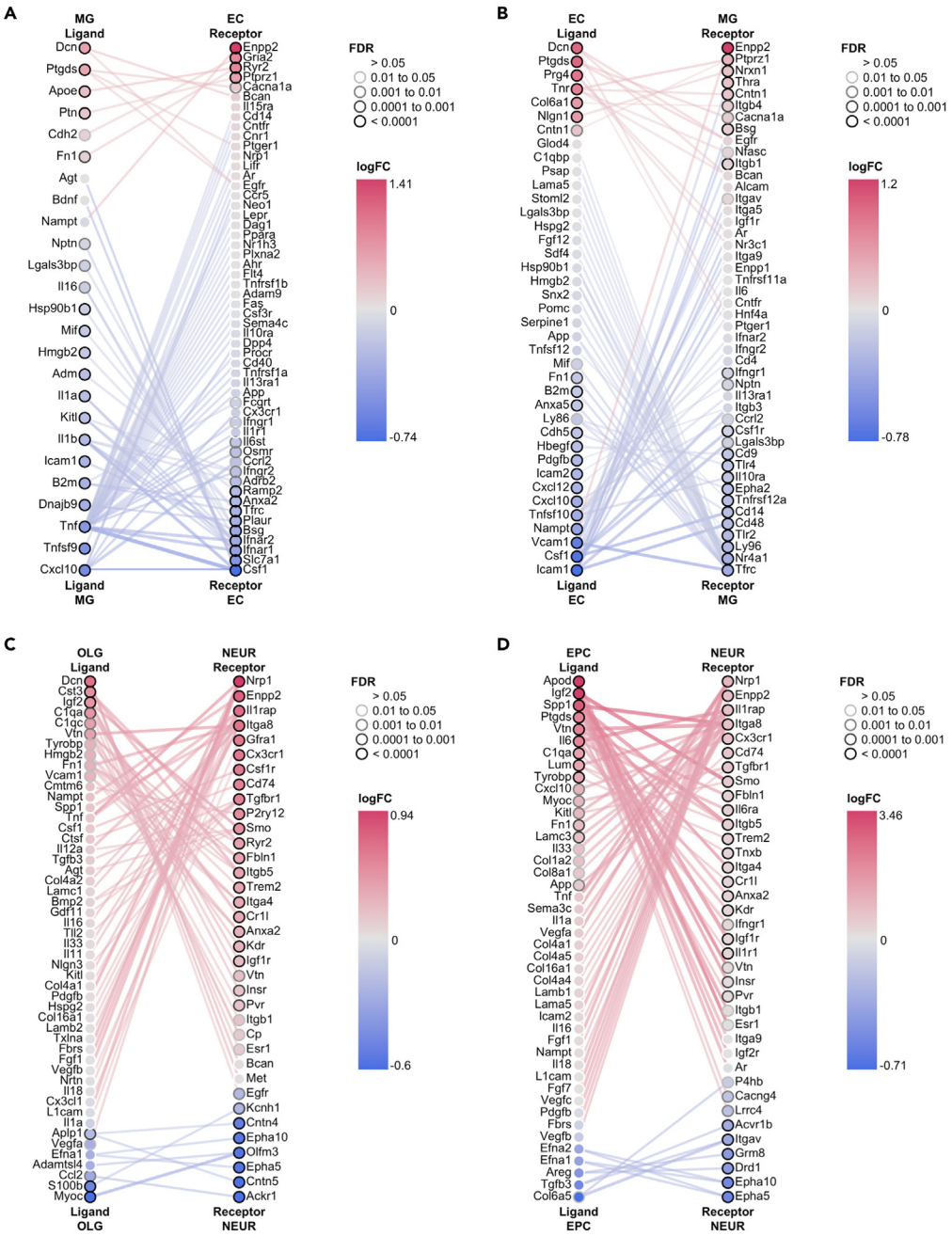

Figure 7. Changes in cell-cell interactions during morphine withdrawal

The comparisons were between With and Dep samples.

(A) Ligands expressed in MG with receptors expressed in EC.

(B) Ligands expressed in EC with receptors expressed in MG.

(C) Ligands expressed in OLG with receptors expressed in NEUR.

(D) Ligands expressed in EPC with receptors expressed in NEUR. See also Figure S11.

Based on the DEG, we conducted GSEA to investigate how different cell types modulated their biological processes. Here, we focused on the immune/inflammation responses that have been shown to influence neuronal activity and have been linked to various neuronal disorders, such as anxiety, depression, and SUD.[6,25,26] Under morphine dependence, notably, microglia were the major cell type mediating an augmented neuroinflammatory response, demonstrated by increased cell activation, enhanced immune and inflammatory responses, promotion of cytokine production, etc. (Figure 4A). Importantly, our data suggest that the amygdala, which is mainly involved in the negative

affect and emotional dysregulation during withdrawal, drive the dependence-associated changes and act as priming events to influence the response to drug withdrawal.

More significant and unexpected changes were observed under the morphine withdrawal condition where two groups of cell types exhibited almost opposite changes in the immune/inflammatory response (Figure 5A). In this study, we applied a spontaneous withdrawal model that mimics human activity. We show that spontaneous withdrawal complements studies that use naloxone precipitated withdrawal models, and also provide additional new information regarding our current understanding of the drug withdrawal process. One of the most recent studies on rat amygdala[38] using laser capture microdissection showed that inflammatory genes, such as Tnf and Il6, remained unchanged with morphine treatment, yet were upregulated in neurons, microglia and astrocytes in the naltrexone-precipitated withdrawal model. In contrast to these studies our scRNA-seq data did not show a similar inflammatory trend in astrocytes, but showed upregulation of Tnf, Icam1, and Cxcl12 in neurons under spontaneous withdrawal condition (Figures 5A and 5D). We show a dampened and down regulated inflammatory response in microglia, macrophages, and endothelial cells in the morphine withdrawal state However, in contrast we show upregulation of inflammatory transcriptomes in the neurons and oligodendrocytes during spontaneous morphine withdrawal (Figure 5A). This bidirectional regulation of the immune response in morphine withdrawal is noteworthy. The reduced immune function in the microglia/immune cells was possibly due to the absence of mu-opioid receptor activation as a consequence of morphine withdrawal, and/or that their cellular activities (immune response is their main function) were compromised as a result of cell death induced by chronic morphine treatment (predicted by GSEA in Figure 4A, and reported by Hu et al. and Xie et al. [23,24]), and/or the signals received from other cells (Figure 7B). At the same time, the reduced immune response in immune cells might directly or indirectly activate the immune response in neurons and oligodendrocytes, such as by enhancing the expressions of chemokines including Icam1 and Cxcl12 to recruit more functional leukocytes and drive an inflammatory milieu that modulate neuronal activity and synaptic transmission (Figure 4C), which consequently can influence the behaviors and emotions during morphine withdrawal. A recent study by Duan et al. showed mitochondria in the amygdala was impaired by chronic stress and mitochondrial loss induced weakening of synapses which resulted in increased anxiety.[39] Highly anxious rats exhibited reduced mitochondrial function in the NAc.[40] In our single-cell data, decreased cellular respiration and mitochondrial function that were suggested in GSEA results were observed in several cell populations, including neurons (Figure 4C). This suggests that mitochondrial dysfunction in the amygdala might greatly affect neurotransmission during withdrawal and as a result promote anxiety-like behavior that accompanies SUD. Our data show for the first time that neuroinflammation is mediated by different cell types under different states during SUD, particularly in microglia cells under dependence state and neurons as well as oligodendrocytes under withdrawal state. Future studies investigating the interaction of inflammatory response with other biological processes will reveal how the biphasic inflammatory response in the microglial cells impact neuronal activity and drive the processes that contribute to SUD.

In addition to studying the biological processes, we analyzed intercellular communications by measuring the ligand-receptor interactions. This is highly important for studies of the brain since the communications between and within glia cell types with surrounding cells including neurons plays pivotal roles in modulating synaptic activity. Of particular interest is the role of inflammatory responses originating in microglial cells and its link to drug dependence and withdrawal cycle. This cell-cell interaction information will help us to discover novel sources and targets of signal transductions that underlie SUD and related co-morbidities.

In summary, our current work has provided a comprehensive dataset of genes, biological pathways and ligand-receptor interactions for all the identified cell types, with a particular emphasis on microglial cells, under both morphine dependence and withdrawal conditions. As a resource for the neuroscience community and to those who study the biology of drug dependence/addiction, our study not only provides more evidence to support the current understanding, in a cell-type specific manner, but also provides novel insight into how different cell populations behave and communicate under different conditions at the molecular level. Since anxiety and depression are comorbidities associated with SUD, our data also provide meaningful information in these fields. Last, the novel findings that are revealed in our data provide clues for future strategies targeting either the genes or pathways in specific cell populations for the prevention or treatment of drug addiction and related neuronal disorders.

Limitations of the study

Our work, as well as recent studies,[7,8,33] benefited from the sensitivity and power of scRNA-seq to study the highly heterogeneous brain tissues and more importantly to investigate cellular changes under different conditions, including drug addiction.[8] One of the limitations of our current study is a single time point of data collection following withdrawal. Future studies aimed at including multiple time points post opioid withdrawal will allow us to link the cycle of dependence and withdrawal to addiction and sustained drug craving. This will also provide more insight into other opioid induced comorbidities such as anxiety and depression-like behaviors, which occur several days or weeks after drug withdrawal.[41,42] It will also be useful to optimize our current single cell dissociation protocol (see STAR methods) to preserve more neurons and oligodendrocytes. Although the cell viabilities of our single cell suspensions were as high as 85–90%, lots of fragile cells were probably lost during the tissue dissociation process, especially neurons. The proportion of neurons and oligodendrocytes in our single-cell data are lower than that in other scRNA-seq datasets[7,8,33,43] where different brain regions and different tissue dissociation procedures were followed. It will be important to explore the ideal protocol so that the scRNA-seq data reflect the actual tissue composition and transcriptomic profiles of each cell type. Future studies, focused on investigating how different brain regions including nucleus accumbens, PFC, etc., and the various subregions in the amygdala contribute to dependence and withdrawal[44] will be an area of great interest. This might be achieved with spatial transcriptomics.[45]

STAR★METHODS

Detailed methods are provided in the online version of this paper and include the following:

- KEY RESOURCES TABLE
- RESOURCE AVAILABILITY
  - Lead contact
  - Materials availability
  - Data and code availability
- EXPERIMENTAL MODEL AND STUDY PARTICIPANT DETAILS
- METHOD DETAILS
  - Withdrawal behavior test
  - Tissue dissociation and single-cell RNA sequencing
  - RNAscope *in situ* hybridization
  - Quick isolation of microglia cells
  - RNA extraction and quantitative real-time PCR
  - Bulk RNA sequencing
- QUANTIFICATION AND STATISTICAL ANALYSIS
  - Raw data processing and clustering
  - Determination of cell identity
  - Analysis of differentially expressed genes (DEG)
  - Pathway analysis and enrichment map
  - Analysis of cell-cell interactions
  - Bulk RNA sequencing and data analysis

SUPPLEMENTAL INFORMATION

Supplemental information can be found online at https://doi.org/10.1016/j.isci.2023.108166.

ACKNOWLEDGMENTS

The authors and their work were supported by National Institutes of Health grants R01 DA044582, R01 DA043252, R01 DA037843, R01 DA047089, DK117576, and R01 DA034582.

AUTHOR CONTRIBUTIONS

Y.Y. and S.R. conceived and designed the study. Y.Y, B.T., J.T., S.M.B., and D.A. conducted the experiment. Y.Y. and W.H. processed the raw scRNA-seq data. Y.Y. analyzed the scRNA-seq data. S.R. supervised the whole study. Y.Y. and S.R. wrote the manuscript. B.T., J.T., and S.M.B. edited the manuscript. All authors reviewed the manuscript and approved the submission.

DECLARATION OF INTERESTS

The authors declare no competing interests.

Received: February 13, 2023
Revised: June 28, 2023
Accepted: October 5, 2023
Published: October 6, 2023

REFERENCES

1. Jones, C.M., Einstein, E.B., and Compton, W.M. (2018). Changes in synthetic opioid involvement in drug overdose deaths in the United States, 2010–2016. JAMA *319*, 1819–1821. https://doi.org/10.1001/jama.2018.2844–1821.
2. Koob, G.F., and Volkow, N.D. (2016). Neurobiology of addiction: a neurocircuitry analysis. Lancet Psychiatr. *3*, 760–773.
3. Albertson, D.N., Schmidt, C.J., Kapatos, G., and Bannon, M.J. (2006). Distinctive profiles of gene expression in the human nucleus accumbens associated with cocaine and heroin abuse. Neuropsychopharmacology *31*, 2304–2312.
4. Korostynski, M., Piechota, M., Kaminska, D., Solecki, W., and Przewlocki, R. (2007). Morphine effects on striatal transcriptome in mice. Genome Biol. *8*, R128.
5. Piechota, M., Korostynski, M., Solecki, W., Gieryk, A., Slezak, M., Bilecki, W., Ziolkowska, B., Kostrzewa, E., Cymerman, I., Swiech, L., et al. (2010). The dissection of transcriptional modules regulated by various drugs of abuse in the mouse striatum. Genome Biol. *11*, R48.
6. Seney, M.L., Kim, S.M., Glausier, J.R., Hildebrand, M.A., Xue, X., Zong, W., Wang, J., Shelton, M.A., Phan, B.N., Srinivasan, C., et al. (2021). Transcriptional alterations in dorsolateral prefrontal cortex and nucleus accumbens implicate neuroinflammation and synaptic remodeling in opioid use disorder. Biol. Psychiatr. *90*, 550–562.
7. Avey, D., Sankararaman, S., Yim, A.K.Y., Barve, R., Milbrandt, J., and Mitra, R.D. (2018). Single-cell RNA-seq uncovers a robust transcriptional response to morphine by glia. Cell Rep. *24*, 3619–3629.e4.

8. Bhattacherjee, A., Djekidel, M.N., Chen, R., Chen, W., Tuesta, L.M., and Zhang, Y. (2019). Cell type-specific transcriptional programs in mouse prefrontal cortex during adolescence and addiction. Nat. Commun. *10*, 4169.
9. Kranzler, H.R., and Liebowitz, N.R. (1988). Anxiety and depression in substance abuse: clinical implications. Med. Clin. *72*, 867–885.
10. Neighbors, B., Kempton, T., and Forehand, R. (1992). Co-occurrence of substance abuse with conduct, anxiety, and depression disorders in juvenile delinquents. Addict. Behav. *17*, 379–386.
11. Miller, D.J., and Fort, P.E. (2018). Heat shock proteins regulatory role in neurodevelopment. Front. Neurosci. *12*, 821.
12. Subramanian, A., Tamayo, P., Mootha, V.K., Mukherjee, S., Ebert, B.L., Gillette, M.A., Paulovich, A., Pomeroy, S.L., Golub, T.R., Lander, E.S., and Mesirov, J.P. (2005). Gene set enrichment analysis: a knowledge-based approach for interpreting genome-wide expression profiles. Proc. Natl. Acad. Sci. USA *102*, 15545–15550.
13. Merico, D., Isserlin, R., Stueker, O., Emili, A., and Bader, G.D. (2010). Enrichment Map: A network-based method for gene-set enrichment visualization and interpretation. PLoS One *5*, e13984.
14. Bachiller, S., Jiménez-Ferrer, I., Paulus, A., Yang, Y., Swanberg, M., Deierborg, T., and Boza-Serrano, A. (2018). Microglia in neurological diseases: a road map to brain-disease dependent-inflammatory response. Front. Cell. Neurosci. *12*, 488.
15. Cahill, C.M., and Taylor, A.M. (2017). Neuroinflammation-a co-occurring phenomenon linking chronic pain and opioid dependence. Curr. Opin. Behav. Sci. *13*, 171–177.
16. Tränkner, D., Boulet, A., Peden, E., Focht, R., Van Deren, D., and Capecchi, M. (2019). A microglia sublineage protects from sex-linked anxiety symptoms and obsessive compulsion. Cell Rep. *29*, 791–799.e3.
17. Stein, D.J., Vasconcelos, M.F., Albrechet-Souza, L., Ceresér, K.M.M., and de Almeida, R.M.M. (2017). Microglial over-activation by social defeat stress contributes to anxiety- and depressive-Like behaviors. Front. Behav. Neurosci. *11*, 207.
18. McKim, D.B., Weber, M.D., Niraula, A., Sawicki, C.M., Liu, X., Jarrett, B.L., Ramirez-Chan, K., Wang, Y., Roeth, R.M., Sucaldito, A.D., et al. (2018). Microglial recruitment of IL-1β-producing monocytes to brain endothelium causes stress-induced anxiety. Mol. Psychiatr. *23*, 1421–1431.
19. Milligan, E.D., and Watkins, L.R. (2009). Pathological and protective roles of glia in chronic pain. Nat. Rev. Neurosci. *10*, 23–36.
20. Wang, X., Loram, L.C., Ramos, K., de Jesus, A.J., Thomas, J., Cheng, K., Reddy, A., Somogyi, A.A., Hutchinson, M.R., Watkins, L.R., and Yin, H. (2012). Morphine activates neuroinflammation in a manner parallel to endotoxin. Proc. Natl. Acad. Sci. USA *109*, 6325–6330.
21. Yang, Y., Sun, Y., Hu, R., Yan, J., Wang, Z., Li, W., and Jiang, H. (2021). Morphine promotes microglial activation by upregulating the EGFR/ERK signaling pathway. PLoS One *16*, e0256870.
22. Hutchinson, M.R., Bland, S.T., Johnson, K.W., Rice, K.C., Maier, S.F., and Watkins, L.R. (2007). Opioid-induced glial activation: mechanisms of activation and implications for opioid analgesia, dependence, and reward. Sci. World J. *7*, 98–111.
23. Hu, S., Sheng, W.S., Lokensgard, J.R., and Peterson, P.K. (2002). Morphine induces apoptosis of human microglia and neurons. Neuropharmacology *42*, 829–836.
24. Xie, N., Li, H., Wei, D., LeSage, G., Chen, L., Wang, S., Zhang, Y., Chi, L., Ferslew, K., He, L., et al. (2010). Glycogen synthase kinase-3 and p38 MAPK are required for opioid-induced microglia apoptosis. Neuropharmacology *59*, 444–451.
25. Heneka, M.T., Carson, M.J., El Khoury, J., Landreth, G.E., Brosseron, F., Feinstein, D.L., Jacobs, A.H., Wyss-Coray, T., Vitorica, J., Ransohoff, R.M., et al. (2015). Neuroinflammation in Alzheimer's disease. Lancet Neurol. *14*, 388–405.
26. Zheng, Z.H., Tu, J.L., Li, X.H., Hua, Q., Liu, W.Z., Liu, Y., Pan, B.X., Hu, P., and Zhang, W.H. (2021). Neuroinflammation induces anxiety- and depressive-like behavior by modulating neuronal plasticity in the basolateral amygdala. Brain Behav. Immun. *91*, 505–518.
27. Davis, S.M., and Pennypacker, K.R. (2018). The role of the leukemia inhibitory factor receptor in neuroprotective signaling. Pharmacol. Ther. *183*, 50–57.
28. Elmore, M.R.P., Najafi, A.R., Koike, M.A., Dagher, N.N., Spangenberg, E.E., Rice, R.A., Kitazawa, M., Matusow, B., Nguyen, H., West, B.L., and Green, K.N. (2014). Colony-stimulating factor 1 receptor signaling is necessary for microglia viability, unmasking a microglia progenitor cell in the adult brain. Neuron *82*, 380–397.
29. Chao, M.V. (2003). Neurotrophins and their receptors: a convergence point for many signalling pathways. Nat. Rev. Neurosci. *4*, 299–309.
30. Ghitza, U.E., Zhai, H., Wu, P., Airavaara, M., Shaham, Y., and Lu, L. (2010). Role of BDNF and GDNF in drug reward and relapse: a review. Neurosci. Biobehav. Rev. *35*, 157–171.
31. Mazzon, C., Zanotti, L., Wang, L., Del Prete, A., Fontana, E., Salvi, V., Poliani, P.L., and Sozzani, S. (2016). CCRL2 regulates M1/M2 polarization during EAE recovery phase. J. Leukoc. Biol. *99*, 1027–1033.
32. Müller, U., Bossy, B., Venstrom, K., and Reichardt, L.F. (1995). Integrin alpha 8 beta 1 promotes attachment, cell spreading, and neurite outgrowth on fibronectin. Mol. Biol. Cell *6*, 433–448.
33. Ximerakis, M., Lipnick, S.L., Innes, B.T., Simmons, S.K., Adiconis, X., Dionne, D., Mayweather, B.A., Nguyen, L., Niziolek, Z., Ozek, C., et al. (2019). Single-cell transcriptomic profiling of the aging mouse brain. Nat. Neurosci. *22*, 1696–1708.
34. Ammon-Treiber, S., Grecksch, G., Stumm, R., Riechert, U., Tischmeyer, H., Reichenauer, A., and Höllt, V. (2004). Rapid, transient, and dose-dependent expression of hsp70 messenger RNA in the rat brain after morphine treatment. Cell Stress Chaperones *9*, 182–197.
35. Ammon, S., Mayer, P., Riechert, U., Tischmeyer, H., and Höllt, V. (2003). Microarray analysis of genes expressed in the frontal cortex of rats chronically treated with morphine and after naloxone precipitated withdrawal. Brain Res. Mol. Brain Res. *112*, 113–125.
36. Nylandsted, J., Gyrd-Hansen, M., Danielewicz, A., Fehrenbacher, N., Lademann, U., Høyer-Hansen, M., Weber, E., Multhoff, G., Rohde, M., and Jäättelä, M. (2004). Heat shock protein 70 promotes cell survival by inhibiting lysosomal membrane permeabilization. J. Exp. Med. *200*, 425–435.
37. Dorion, S., and Landry, J. (2002). Activation of the mitogen-activated protein kinase pathways by heat shock. Cell Stress Chaperones *7*, 200–206.
38. O'Sullivan, S.J., Malahias, E., Park, J., Srivastava, A., Reyes, B.A.S., Gorky, J., Vadigepalli, R., Van Bockstaele, E.J., and Schwaber, J.S. (2019). Single-cell glia and neuron gene expression in the central amygdala in opioid withdrawal suggests inflammation with correlated gut dysbiosis. Front. Neurosci. *13*, 665.
39. Duan, K., Gu, Q., Petralia, R.S., Wang, Y.X., Panja, D., Liu, X., Lehmann, M.L., Zhu, H., Zhu, J., and Li, Z. (2021). Mitophagy in the basolateral amygdala mediates increased anxiety induced by aversive social experience. Neuron *109*, 3793–3809.e8.
40. Hollis, F., van der Kooij, M.A., Zanoletti, O., Lozano, L., Cantó, C., and Sandi, C. (2015). Mitochondrial function in the brain links anxiety with social subordination. Proc. Natl. Acad. Sci. USA *112*, 15486–15491.
41. Shahroodi, A., Mohammadi, F., Vafaei, A.A., Miladi-Gorji, H., Bandegi, A.R., and Rashidy-Pour, A. (2020). Impact of different intensities of forced exercise on deficits of spatial and aversive memory, anxiety-like behavior, and hippocampal BDNF during morphine abstinence period in male rats. Metab. Brain Dis. *35*, 135–147.
42. Zan, G.Y., Wang, Y.J., Li, X.P., Fang, J.F., Yao, S.Y., Du, J.Y., Wang, Q., Sun, X., Liu, R., Shao, X.M., et al. (2021). Amygdalar κ-opioid receptor-dependent upregulating glutamate transporter 1 mediates depressive-like behaviors of opioid abstinence. Cell Rep. *37*, 109913.
43. Wu, Y.E., Pan, L., Zuo, Y., Li, X., and Hong, W. (2017). Detecting activated cell populations using single-cell RNA-seq. Neuron *96*, 313–329.e6.
44. Yang, Y., and Wang, J.Z. (2017). From structure to behavior in basolateral amygdala-hippocampus circuits front. Neural Circuits *11*, 86.
45. Vickovic, S., Eraslan, G., Salmén, F., Klughammer, J., Stenbeck, L., Schapiro, D., Äijö, T., Bonneau, R., Bergenstråhle, L., Navarro, J.F., et al. (2019). High-definition spatial transcriptomics for in situ tissue profiling. Nat. Methods *16*, 987–990.
46. Taylor, J.R., Punch, L.J., and Elsworth, J.D. (1998). A comparison of the effects of clonidine and CNQX infusion into the locus coeruleus and the amygdala on naloxone-precipitated opiate withdrawal in the rat. Psychopharmacology *138*, 133–142.
47. Zapala, M.A., Hovatta, I., Ellison, J.A., Wodicka, L., Del Rio, J.A., Tennant, R., Tynan, W., Broide, R.S., Helton, R., Stoveken, B.S., et al. (2005). Adult mouse brain gene expression patterns bear an embryologic imprint. Proc. Natl. Acad. Sci. USA *102*, 10357–10362.
48. Saxena, A., Wagatsuma, A., Noro, Y., Kuji, T., Asaka-Oba, A., Watahiki, A., Gurnot, C., Fagiolini, M., Hensch, T.K., and Carninci, P. (2012). Trehalose-enhanced isolation of neuronal sub-types from adult mouse brain. Biotechniques *52*, 381–385.
49. Satija, R., Farrell, J.A., Gennert, D., Schier, A.F., and Regev, A. (2015). Spatial reconstruction of single-cell gene expression data. Nat. Biotechnol. *33*, 495–502.
50. Hao, Y., Hao, S., Andersen-Nissen, E., Mauck, W.M., 3rd, Zheng, S., Butler, A., Lee, M.J.,

Wilk, A.J., Darby, C., Zager, M., et al. (2021). Integrated analysis of multimodal single-cell data. Cell *184*, 3573–3587.e29.
51. Stuart, T., Butler, A., Hoffman, P., Hafemeister, C., Papalexi, E., Mauck, W.M., 3rd, Hao, Y., Stoeckius, M., Smibert, P., and Satija, R. (2019). Comprehensive integration of single-cell data. Cell *177*, 1888–1902.e21.
52. Marques, S., Zeisel, A., Codeluppi, S., van Bruggen, D., Mendanha Falcão, A., Xiao, L., Li, H., Häring, M., Hochgerner, H., Romanov, R.A., et al. (2016). Oligodendrocyte heterogeneity in the mouse juvenile and adult central nervous system. Science *352*, 1326–1329.
53. Hammond, T.R., Dufort, C., Dissing-Olesen, L., Giera, S., Young, A., Wysoker, A., Walker, A.J., Gergits, F., Segel, M., Nemesh, J., et al. (2019). Single-cell RNA sequencing of microglia throughout the mouse lifespan and in the Injured brain reveals complex cell-state changes. Immunity *50*, 253–271.e6.
54. Vanlandewijck, M., He, L., Mäe, M.A., Andrae, J., Ando, K., Del Gaudio, F., Nahar, K., Lebouvier, T., Laviña, B., Gouveia, L., et al. (2018). A molecular atlas of cell types and zonation in the brain vasculature. Nature *554*, 475–480.
55. Tasic, B., Menon, V., Nguyen, T.N., Kim, T.K., Jarsky, T., Yao, Z., Levi, B., Gray, L.T., Sorensen, S.A., Dolbeare, T., et al. (2016). Adult mouse cortical cell taxonomy revealed by single cell transcriptomics. Nat. Neurosci. *19*, 335–346.
56. Jordão, M.J.C., Sankowski, R., Brendecke, S.M., Sagar, Locatelli, G., Tai, Y., Tay, T.L., Schramm, E., Armbruster, S., Hagemeyer, N., et al. (2019). Single-cell profiling identifies myeloid cell subsets with distinct fates during neuroinflammation. Science *363*, 6425.
57. Kalish, B.T., Cheadle, L., Hrvatin, S., Nagy, M.A., Rivera, S., Crow, M., Gillis, J., Kirchner, R., and Greenberg, M.E. (2018). Single-cell transcriptomics of the developing lateral geniculate nucleus reveals insights into circuit assembly and refinement. Proc. Natl. Acad. Sci. USA *115*, E1051–E1060.
58. Zhang, Y., Chen, K., Sloan, S.A., Bennett, M.L., Scholze, A.R., O'Keeffe, S., Phatnani, H.P., Guarnieri, P., Caneda, C., Ruderisch, N., et al. (2014). An RNA-sequencing transcriptome and splicing database of glia, neurons, and vascular cells of the cerebral cortex. J. Neurosci. *34*, 11929–11947.
59. Han, X., Wang, R., Zhou, Y., Fei, L., Sun, H., Lai, S., Saadatpour, A., Zhou, Z., Chen, H., Ye, F., et al. (2018). Mapping the mouse cell atlas by Microwell-Seq. Cell *172*, 1091–1107.e17.
60. Campbell, J.N., Macosko, E.Z., Fenselau, H., Pers, T.H., Lyubetskaya, A., Tenen, D., Goldman, M., Verstegen, A.M.J., Resch, J.M., McCarroll, S.A., et al. (2017). A molecular census of arcuate hypothalamus and median eminence cell types. Nat. Neurosci. *20*, 484–496.
61. Llorens-Bobadilla, E., Zhao, S., Baser, A., Saiz-Castro, G., Zwadlo, K., and Martin-Villalba, A. (2015). Single-cell transcriptomics reveals a population of dormant neural stem cells that become activated upon brain injury. Cell Stem Cell *17*, 329–340.
62. Liu, Y., Han, S.S.W., Wu, Y., Tuohy, T.M.F., Xue, H., Cai, J., Back, S.A., Sherman, L.S., Fischer, I., and Rao, M.S. (2004). CD44 expression identifies astrocyte-restricted precursor cells. Dev. Biol. *276*, 31–46.
63. Zeisel, A., Muñoz-Manchado, A.B., Codeluppi, S., Lönnerberg, P., La Manno, G., Juréus, A., Marques, S., Munguba, H., He, L., Betsholtz, C., et al. (2015). Brain structure. Cell types in the mouse cortex and hippocampus revealed by single-cell RNA-seq. Science *347*, 1138–1142.
64. Batiuk, M.Y., Martirosyan, A., Wahis, J., de Vin, F., Marneffe, C., Kusserow, C., Koeppen, J., Viana, J.F., Oliveira, J.F., Voet, T., et al. (2020). Identification of region-specific astrocyte subtypes at single cell resolution. Nat. Commun. *11*, 1220.
65. Robinson, M.D., McCarthy, D.J., and Smyth, G.K. (2010). edgeR: a Bioconductor package for differential expression analysis of digital gene expression data. Bioinformatics *26*, 139–140.
66. Lun, A.T.L., Chen, Y., and Smyth, G.K. (2016). It's DE-licious: a recipe for differential expression analyses of RNA-seq experiments using quasi-likelihood methods in edgeR. Methods Mol. Biol. *1418*, 391–416.
67. Soneson, C., and Robinson, M.D. (2018). Bias, robustness and scalability in single-cell differential expression analysis. Nat. Methods *15*, 255–261.
68. Reimand, J., Isserlin, R., Voisin, V., Kucera, M., Tannus-Lopes, C., Rostamianfar, A., Wadi, L., Meyer, M., Wong, J., Xu, C., et al. (2019). Pathway enrichment analysis and visualization of omics data using g:Profiler, GSEA, Cytoscape and EnrichmentMap. Nat. Protoc. *14*, 482–517.
69. Kucera, M., Isserlin, R., Arkhangorodsky, A., and Bader, G.D. (2016). AutoAnnotate: a Cytoscape app for summarizing networks with semantic annotations. F1000Res. *5*, 1717.
70. Bolger, A.M., Lohse, M., and Usadel, B. (2014). Trimmomatic: A flexible trimmer for Illumina Sequence Data. Bioinformatics *30*, 2114–2120.
71. Dobin, A., Davis, C.A., Schlesinger, F., Drenkow, J., Zaleski, C., Jha, S., Batut, P., Chaisson, M., and Gingeras, T.R. (2013). STAR: ultrafast universal RNA-seq aligner. Bioinformatics *29*, 15–21.
72. Liao, Y., Smyth, G.K., and Shi, W. (2019). The R package Rsubread is easier, faster, cheaper and better for alignment and quantification of RNA sequencing reads. Nucleic Acids Res. *47*, e47.
73. Love, M.I., Huber, W., and Anders, S. (2014). Moderated estimation of fold change and dispersion for RNA-seq data with DESeq2. Genome Biol. *15*, 550.

STAR★METHODS

KEY RESOURCES TABLE

REAGENT or RESOURCE	SOURCE	IDENTIFIER
Antibodies		
CD11b+ MicroBeads	Miltenyi Biotec	Cat No. 130-093-636
CD45-PercP-Cy5.5	BioLegend	Cat No. 103132
Cd11b-APC	BioLegend	Cat No. 101212
Chemicals, peptides, and recombinant proteins		
Morphine sulfate	Sigma-Aldrich	Cat No. 1448005
HBSS, calcium, magnesium, no phenol red	Thermo Fisher	Cat No. 14025092
Trehalose	Sigma-Aldrich	Cat No. T0167
Tissue-Tek® O.C.T. Compound	Sakura Finetek	Cat No. 4583
Critical commercial assays		
Papain Dissociation System	Worthington Biochemical	Cat No. LK003182
Chromium Next GEM Automated Single Cell 3′ cDNA Kit	10X Genomics	Cat No. 1000424
Chromium Next GEM Automated Single Cell 3′ Library and Gel Bead Kit	10X Genomics	Cat No. 1000147
RNAscope Multiplex Fluorescent Manual Assay kit	Advanced Cell Diagnostics	Cat No. 323136
RNeasy Mini Kit	QIAGEN	Cat No. 74104
SuperScript™ IV First-Strand Synthesis System	Invitrogen	Cat No. 18091050
SMART-Seq v4 Ultra Low Input RNA Kit	TaKaRa Bio	Cat No. 634894
Nextera XT DNA Library Preparation Kit	Illumina	Cat No. FC-131-1024
Deposited data		
Raw single-cell RNA sequencing data and the count matrices	This paper	Gene Expression Omnibus (GEO) accession number GSE207128
Experimental models: Organisms/strains		
Mouse/C57BL/6J male	The Jackson Laboratory	https://www.jax.org/strain/000664
Oligonucleotides		
Probes against Tmem119	Advanced Cell Diagnostics	Cat No. 472901
Probes against Ccl2	Advanced Cell Diagnostics	Cat No. 311791
Probes against Dnaja1	Advanced Cell Diagnostics	Cat No. 454351
Software and algorithms		
Cell Ranger (v.6.1)	10X Genomics	https://support.10xgenomics.com/single-cell-gene-expression/software/pipelines/latest/release-notes
R (v.4.1)	R Core Team (2021). R: A language and environment for statistical computing. R Foundation for Statistical Computing, Vienna, Austria.	https://www.R-project.org/
Seurat (v4.0)	Satija, R. et al.[49]	https://satijalab.org/seurat/
edgeR (v.3.32)	Robinson, M. D. et al.[65]	https://bioconductor.org/packages/release/bioc/html/edgeR.html
GSEA software (v.4.1)	UC San Diego and Broad Institute	https://www.gsea-msigdb.org/gsea/index.jsp

(*Continued on next page*)

Continued

REAGENT or RESOURCE	SOURCE	IDENTIFIER
Cytoscape software (v.3.9)	U.S. National Institute of General Medical Sciences (NIGMS)	https://cytoscape.org
CCInx (v.0.5)	Ximerakis, M. et al.[33]	https://github.com/BaderLab/CCInx
ImageJ	National Institutes of Health and the Laboratory for Optical and Computational Instrumentation	https://ImageJ.nih.gov/ij/download.html
Trimmomatic (v.0.36)	Bolger, A. M. et al.[70]	https://github.com/timflutre/trimmomatic
STAR aligner (v.2.5.2b)	Dobin, A. et al.[71]	https://github.com/alexdobin/STAR
FeatureCounts from the Subread (v.1.5.2)	Liao, Y. et al.[72]	https://subread.sourceforge.net/
DESeq2 (v.1.34.0)	Love, M. I. et al.[73]	https://bioconductor.org/packages/release/bioc/html/DESeq2.html

RESOURCE AVAILABILITY

Lead contact

Further information and requests for resources should be directed to the lead contact, Sabita Roy (Sabita.Roy@miami.edu).

Materials availability

This study did not generate new unique reagents.

Data and code availability

- The raw single-cell sequencing data and the count matrices are available through Gene Expression Omnibus (GEO) under the accession number GSE207128.
- This paper does not use customized code and does not report original code.
- Any additional information required to reanalyze the data reported in this paper is available from the lead contact upon request.

EXPERIMENTAL MODEL AND STUDY PARTICIPANT DETAILS

Eight-week-old C57BL/6J male mice were purchased from Jackson Laboratories (Bar Harbor, ME, USA) (https://www.jax.org/strain/000664). Animal maintenance and procedures were conducted according to the Institutional Animal Care and Use Committee policies at the University of Miami. Mice were injected with morphine sulfate (15 mg/kg) intraperitoneally (IP) twice daily (every 12 h) for 7 days. Mice in the Dep group were sacrificed 3 h after last injection and mice in the With group were sacrificed 24 h after last injection. Mice in the Naive group received no treatment. The detailed drug treatment plan was shown in Figure S1A.

METHOD DETAILS

Withdrawal behavior test

Withdrawal behavior was monitored 24 h after the last morphine injection to evaluate both the presence and severity of withdrawal symptoms. Mice were placed in a plexiglass chamber for 15 min and their behavior was recorded on a video camera. The videos were scored and verified by a blind observer for withdrawal symptoms that were described previously.[46] In this study, symptoms of withdrawal were evaluated on the frequency of symptoms including shaking (shaking of head or the entire body), jumping (raising all four paws off the ground rapidly) and grooming (using limbs to manipulate head or body). This resulted in a quantifiable score of the withdrawal symptoms, in which a higher withdrawal score signified higher severity of withdrawal. These withdrawal scores were compared between the With and Naive groups.

Tissue dissociation and single-cell RNA sequencing

Three batches of experiments were conducted, and each batch included one Naive, Dep and With group. Thus, nine independent biological samples were processed. Amygdala dissection and tissue dissociation were performed at the same time period (10a.m.–12p.m.) for all the samples to limit circadian variation. The widely used Papain Dissociation System (Worthington Cat No. LK003182) was modified based on other published protocols[8,33] so that single cell solutions with high cell viability (~90%) could be acquired within 2 h (Figure S2A). Briefly, after mice were sacrificed brains were immediately dissected and transferred into ice-cold HBSS. The amygdalae were dissected from 4 to 5 mice according to the previous protocol[47] and were pooled together. The tissues were cut into small pieces and incubated in 2 mL pre-warmed papain solution (EBSS containing approximately 20 units/mL papain and 0.005% DNase) at 30°C for 45 min with gentle constant agitation. After the incubation, all the following procedures were performed on ice. The mixture was triturated gently with a fire polished 2 mL Pasteur

glass pipette and the supernatant were transferred carefully to a fresh tube. 2 mL of EBSS containing the albumin ovomucoid inhibitor was added to the remaining tissues, which was triturated gently with another fire polished 2 mL Pasteur glass pipette and the supernatant was transferred. This step was repeated one more time. The resulted 6 mL supernatant containing single cells were pooled together and the cell clusters/tissue debris were removed by serial filtration through pre-wetted 70 μm and 40 μm cell strainers. The single cell suspension was centrifuged at 220 g for 7 min at 4°C. The cells were then washed in 10 mL PBS containing 0.04% BSA twice, after which the cells were resuspended in PBS containing 0.04% BSA. 10 μL aliquots were stained with Trypan Blue and cell numbers were counted three times for each sample. During the whole procedure, 5% (w/v) trehalose (Sigma Aldrich Cat No. T0167) was added in the buffers to ensure higher cell viability.[48]

After dissociation, cell suspensions were diluted to 1,000–1,200 cells/μL with PBS containing 0.04% BSA. For every sample, 16,500 cells were loaded into a Chromium Single Cell 3′ Chip (10X Genomics) and processed according to the manufacturer's protocol. scRNA-seq libraries were prepared with the Chromium Single Cell 3′ GEM, Library & Gel Bead kits v3.1 (10X Genomics). Libraries were pooled and sequenced on the NovaSeq6000 instrument (Illumina).

RNAscope *in situ* hybridization

RNAscope in situ hybridization was performed on fresh-frozen brain tissue from 15 mice (5 Naive, 5 Dep and 5 With). Brains were harvested immediately after the mice were sacrificed. The coronal section (~2 mm) containing the amygdala were flash-frozen in OCT (Tissue Tek) and were saved at −80°C until further processing. 14 μm coronal sections were cut at −20°C. Multi-channel fluorescence *in situ* hybridization was performed using the RNAscope Multiplex Fluorescent Manual Assay kit (Advanced Cell Diagnostics (ACD)) following the manufacturer's protocol. Regions of the amygdala were selected according to the Allen Mouse Brain Atalas (https://portal.brain-map.org). Probes against *Tmem119* (ACD Cat No. 472901), *Ccl2* (ACD Cat No. 311791) and *Dnaja1* (ACD Cat No. 454351) were used. The RNAscope slides were imaged on a Leica LAS X microscope system. Image files were processed and analyzed in ImageJ software. Briefly, we located *Tmem19* positive cells and drew the cell boundaries based on DAPI-positive nuclei. We used the ImageJ analyze particles tool to quantify the number of puncta per cell. Only puncta with the size above diameter of 2 pixels would be counted.

Quick isolation of microglia cells

In order to collect as many microglia cells as possible and process the cells quickly, we followed the approach of using magnetic beads to isolate microglia cells from the amygdala tissues. Briefly, for each experiment group the amygdalae were dissected from 4 to 5 mice and were pooled together. The single cell suspension was obtained following the method as described in "tissue dissociation and single-cell RNA sequencing". Then the cells were incubated with $CD11b^{+}$ MicroBeads (Miltenyi Biotec Cat No. 130-093-636) for 15 min in the dark at 4°C, after which the cells were washed with 1 mL of cold washing buffer (PBS containing 0.5% BSA) and were centrifuged at 300 g for 5 min at 4°C. The cells were resuspended with 500 μL washing buffer and loaded on a pre-rinsed MS column on the OctoMACS Separator. The column was washed with 1 mL washing buffer. After the column was removed from the separator, 1 mL washing buffer was added to the column and the magnetically labeled cells were immediately flushed out to the collection tube. The cells were centrifuged at 300 g for 5 min at 4°C and were processed immediately for RNA extraction.

To investigate the purity of the isolated microglial population, the isolated cells were stained with antibodies CD45-PercP-Cy5.5 (BioLegend Cat No. 103132) and Cd11b-APC (BioLegend Cat No. 101212). Flow cytometry was performed and the data showed the percentage of CD45+/CD11b+ cells is over 90% (Figure S9A).

RNA extraction and quantitative real-time PCR

Total RNA was extracted from the isolated microglia cells with the RNeasy Mini Kit (Qiagen Cat No. 74104) following the manufacturer's protocol. cDNA was synthesized with SuperScript IV First-Strand Synthesis System (Invitrogen Cat No. 18091050) and was used as the template for quantitative real-time PCR in the LightCycler 480 System (Roche, US).

Bulk RNA sequencing

Total RNA was extracted from the isolated microglia cells with the RNeasy Mini Kit (Qiagen Cat No. 74104) following the manufacturer's protocol. Reverse transcription and cDNA amplification were performed with the SMART-Seq v4 Ultra Low Input RNA Kit (TaKaRa Bio). Libraries were constructed using the Illumina Nextera XT kit. Sequencing was performed on the Illumina HiSeq 2500.

QUANTIFICATION AND STATISTICAL ANALYSIS

Raw data processing and clustering

Cell Ranger (v.6.1) (10X Genomics) was used to perform de-multiplexing, barcode processing and generate the single cell gene expression matrix with the default parameters.

Initial processing and visualization of the scRNA-seq data were performed with the Seurat (v.4.0) package[49,50] in R (v.4.1). Our initial dataset with nine samples together contained 121,856 cells. For initial quality-control, we filtered the cells with the following parameters: maximum percentage of mitochondrial RNA = 20% (to remove potential dead cells), minimum number of nFeature_RNA = 250 and minimum number of nCount_RNA = 500 (to remove debris), maximum number of nFeature_RNA = 6,000 and maximum number of nCount_RNA = 30,000 (to

exclude potential doublets and outliers). We also removed any genes that were only expressed in fewer than 5 cells. With the remaining 82,528 cells we did an initial clustering. To minimize potential batch effect and to perform comparative scRNA-seq analysis across experimental conditions, we applied the Seurat integration procedure.[51] Briefly, the data from each sample were log normalized and scaled to 10,000 transcripts per cell, and the function FindVariableGene was used to identify variable features for each sample independently. The function SelectIntegrationFeatures was then used to select features that are repeatedly variable across samples, after which the anchors were identified using the FindIntegrationAnchors function. Then these anchors were used to integrate the nine samples together with the function IntegrateData. The integrated data were scaled to find the top 30 principal components (PCs) which were used to identify cell clusters by using the function FindNeighbors followed by FindClusters with the resolution as 1.0. This procedure resulted in 46 clusters and the color-coded clusters were visualized with the UMAP plot Figure S3A).

To determine the cell types for these initial 46 clusters, we first used the function FindAllMarkers to search for the top differential markers for each cluster, which were then paired with multiple cell-type specific/enriched marker genes (described in the next section). The clusters being assigned to the same cell type were combined and 22 clusters were generated, including two unrecognized clusters (Figure S3B). As the transcriptional profiles shown in Figure S3C, one of the unrecognized clusters expressed both astrocyte marker (*Gja1*) and oligodendrocyte marker (*Mbp*) and the other expressed both neuron marker (*Syt1*) and microglial marker (*Tmem119*). These clusters were likely doublet artifacts arising from the co-capture of multiple cells in one droplet, yet it was also possible they were novel cell types that have not been identified. It will be interesting to investigate these cells in future studies. For our current data analysis, we removed these two clusters. Additionally, we filtered out the cells that belong to meningeal tissue that we didn't remove at the initial dissection step for the sake of fast sample processing. These cells included epithelial cells (EPIC), arachnoid barrier cells (ABC) as well as vascular and leptomeningeal cells (VLMC) (Figure S3B). Finally, 77,957 cells representing 17 clusters (Figure 1B; Table S3) with data for 23,057 genes were retained in our dataset for subsequent analysis. For the final dataset, the average number of detected genes, number of UMI counts and percentage of mitochondrial RNA were 2,407.8, 6,508.1, and 9.27% respectively. Other sequencing metrics about each sample, experiment group, batch, and cluster were summarized in Table S2, and shown in Figures S2–S4.

Determination of cell identity

Cell-type specific/enriched marker genes that have been described before to determine cell identity were used: *Gja1*[43] for ASC, *Pdgfra*[52] for OPC, *Tmem119*[53] for MG, *Cldn5*[54] for EC, *Syt1*[55] for NEUR, *Cldn11*[51] and *Mobp*[8] for OLG, *Pf4*[56] for MAC, *Vtn*[57] for PC, *Enpp6*[58] for NFOLG, *Acta2*[53] for VSMC, *Cd74* and *Cd209a*[59] for DC, *Ccdc153*[60] for EPC, *Thbs4*[61] for NSC, *Cd44*[62] for ARP, *Top2a* and *Cdk1*[33] for NRP, *Cd3d* for Tcells, *S100a9*[58] for NEUT, *Ttr*[63] for EPIC; *Slc6a13*[33] for VLMC; *Slc47a1*[33] for ABC. For the neuron and astrocyte sub-clustering, the similar procedures were conducted, and the identification of their subtypes was based on reported neuron[8,33,64] or astrocyte[64] subtype marker genes respectively.

Analysis of differentially expressed genes (DEG)

To identify the DEG compared between experiment groups (Dep vs. Naive, With vs. Dep), we used the edgeR (v.3.32) package[65] in R (v.4.1) and the analysis was performed on single-cell basis. edgeR generates logFC (with the base as 2), p value and p values adjusted by FDR across all the tested genes. Specifically, we used the edgeRQLFDetRate method which is based on quasi-likelihood F-test, resulting in more conservative and rigorous type I error rate control,[66] and has been shown to perform better than other methods for DEG analysis in scRNA-seq data.[67] With this method we were able to detect significant subtle transcriptional changes in the clusters that had large number of cells, while in relatively small cell populations it was more conservative to identify the DEG with much higher fold changes (Figures 2A and 2B; Tables S5 and S6).

Pathway analysis and enrichment map

Gene Set Enrichment Analysis (GSEA) [12] was used to analyze the changes of biological processes or pathways between experiment groups (Dep vs. Naive, With vs. Dep). We used the GSEA software (v.4.1) that was developed and maintained by UC San Diego and Broad Institute.[12] Pathway analysis and visualization were conducted following the protocol described by Reimand et al.[68] Briefly, for each comparison between experiment groups a ranked gene list was generated for each cell population. These ranked gene lists were used as input, and two databases (GeneOntology and Reactome) were used as references for the GSEA analysis. 1000 permutations were performed. Only gene sets with p value <0.05 and FDR q value <0.25 were considered as significantly enriched. Normalized Enrichment Score (NES) was used for examining gene set enrichment. A positive NES indicated upregulation while negative NES indicated downregulation.

Pathway network visualization was carried out with the EnrichmentMap application (v.3.3) [13] in Cytoscape software (v.3.9). Only the gene sets (p value <0.05 and FDR q value <0.15) for GO biological processes were mapped. Pathways were shown as nodes that were connected with edges if the pathways shared many genes. Nodes were colored by NES, and edges were sized on the basis of number of genes shared by the connected pathways. Nodes were manually laid out to form a clearer picture. Gene sets that represented the similar pathways were grouped together and labeled using the AutoAnnotate application (v.1.3).[69] Individual gene set labels were removed for clarity.

Analysis of cell-cell interactions

The cell-cell communication mediated by ligand-receptor interactions were analyzed using the CCInx (v.0.5) package[33] in R (v.4.1). The ligand-receptor interaction dataset is available at https://baderlab.org/CellCellInteractions. To study the changes of these interactions under morphine dependence or withdrawal conditions, the DEG being analyzed by edgeR were used to build the networks between cell types. In these networks, ligands or receptors in the denoted cell type were represented by the nodes which were colored by the log2FC. Node borders indicated the FDR value of the DEG. Edges represent ligand-receptor interactions. Edge color indicated the sum of scaled differential expression magnitudes from the ligand node and receptor node.

Bulk RNA sequencing and data analysis

Sequence reads were trimmed to remove possible adapter sequences and nucleotides with poor quality using Trimmomatic (v.0.36).[70] The trimmed reads were mapped to the Mus musculus GRCm38 reference genome using the STAR aligner (v.2.5.2b).[71] Unique gene hit counts were calculated by using featureCounts from the Subread package (v.1.5.2).[72] Downstream differential expression analysis was performed using DESeq2 package (v.1.34.0).[73] The Wald test was used to generate p values and log2 fold changes. Genes with an adjusted p value <0.05 were called as differentially expressed genes for each comparison.